Regenerative growth is constrained by *brain tumor* to ensure proper patterning in *Drosophila*

Short Title: The role of *brain tumor* in imaginal disc regeneration

Syeda Nayab Fatima Abidi[1], Felicity Ting-Yu Hsu[1], and Rachel K. Smith-Bolton[1,2,*]

[1] Department of Cell and Developmental Biology, University of Illinois at Urbana-Champaign, Urbana, IL 61801, USA

[2]Carle R. Woese Institute for Genomic Biology, University of Illinois at Urbana-Champaign, Urbana, IL, 61801, USA

* rsbolton@illinois.edu

Abstract

Some animals respond to injury by inducing new growth to regenerate the lost structures. This regenerative growth must be carefully controlled and constrained to prevent overgrowth and to allow correct organization of the regenerating tissue. However, the factors that restrict regenerative growth have not been identified. Using a genetic ablation system in the *Drosophila* wing imaginal disc, we have identified one mechanism that constrains regenerative growth, impairment of which also leads to erroneous patterning of the final appendage. Regenerating discs with reduced levels of the RNA-regulator Brain tumor (Brat) exhibit enhanced regeneration, but produce adult wings with disrupted margins that are missing extensive tracts of sensory bristles. In these mutants, aberrantly high expression of the pro-growth factor Myc and its downstream targets likely contributes to this loss of cell-fate specification. Thus, Brat constrains the expression of pro-regeneration genes and ensures that the regenerating tissue forms the proper final structure.

Author Summary

While much has been published about the signals that stimulate regeneration, the mechanisms that constrain and/or terminate regeneration have not been well characterized. Thus, we do not understand what limits may exist on the rate of

regenerative growth, what mechanisms constrain regeneration, and what the consequences might be of enhancing regrowth. Here, we detail our discovery and characterization of a mechanism that constrains regeneration, and the deleterious effects of reducing that constraint. In this manuscript, we describe our identification of the RNA regulator Brat as a factor that constrains regenerative growth. Without this constraint on regenerative growth, patterning mistakes occur leading to a malformed regenerated structure. We demonstrate that the patterning errors are not due to faster growth itself, but are due to the overexpression of the pro-growth transcription factor Myc.

Introduction

Regeneration is the remarkable process by which some organisms replace tissues and organs after damage such that both morphology and function are restored. Complete regeneration requires several steps to occur correctly including wound healing, cell proliferation, and proper patterning and cell-fate specification in the newly formed tissue. The degree of regenerative capacity varies among different species, ranging from whole-body regeneration in hydra and planaria to limited tissue regeneration in mammals. Work in several model organisms has identified signaling pathways and molecular mechanisms that are important for initiating and executing regenerative growth after tissue damage, including JNK signaling (1–5), JAK/STAT signaling (6–8), EGFR signaling (9–12), Hippo signaling (13–17), Wnt signaling (18–24), and Myc (23,25). Many of these mechanisms are also important during normal development, and the process of regeneration was traditionally thought to be a redeployment of earlier

43 developmental steps (3,9,25–29). However, recent evidence suggests that regeneration
44 is not a simple reiteration of development but can employ regeneration-specific
45 regulatory mechanisms (3,25,30–34). Indeed, faithful regeneration likely requires
46 additional mechanisms, since regrowth happens in the presence of wound-response
47 signaling and in a developed juvenile or adult organism. Additionally, pro-growth
48 pathways that are used during normal development are often activated in new ways and
49 at higher strengths in the regenerating tissue (2,7,15,23). These augmented pro-growth
50 signals must be constrained as regeneration progresses to prevent overgrowth and to
51 enable re-establishment of pattern and cell-fate specification. Thus, growth suppressors
52 and additional patterning factors are likely used to terminate regeneration and allow
53 differentiation (35). However, despite our understanding of the pro-growth signals
54 needed for regeneration, we do not yet know what factors exist in different model
55 organisms to restrain growth and promote re-patterning of regenerating tissue.

56

57 *Drosophila melanogaster* imaginal discs, precursors of adult fly appendages, are simple
58 columnar epithelia that have well-characterized, complex expression of patterning
59 genes that determine cell-fate specification. Imaginal discs undergo regeneration after
60 damage (36), and we have previously used a genetic ablation system to study
61 patterning in the regenerating tissue (23,32). Here we identify the RNA-regulator Brain
62 tumor (Brat) as a key constraint on regenerative growth that ensures proper formation of
63 the regenerated structure. Brat is a member of the TRIM- (tripartite motif containing)-
64 NHL (NCL-1, HT2A, and LIN-41) family of proteins and functions as a translational
65 repressor by binding to its target RNAs either independently or in a complex with

66 Pumilio and Nanos (37–39). It acts as a potent differentiation factor and tumor
67 suppressor in neural and ovarian germline stem cell lineages (40–43). Human and
68 mouse orthologs of Brat, TRIM3 and TRIM32 respectively, also possess tumor-
69 suppressor activity in glioblastomas and are required for neuronal and muscle
70 differentiation (44–47).

71

72 We show that regenerating wing imaginal discs with reduced levels of Brat regenerate
73 better than controls, but the resulting adult wings have a disrupted margin. The margin
74 loses some of the characteristic sensory bristles and veins, demonstrating an error in
75 cell-fate specification. Importantly, these phenotypes are regeneration-specific, as they
76 are not observed in the mutant animals after normal development. The enhanced
77 regeneration is due to increased expression of the growth regulators Myc and Wingless
78 as well as upregulation of *ilp8,* which delays metamorphosis and allows the damaged
79 tissue more time to regenerate. Intriguingly, this seemingly beneficial elevated Myc
80 expression can also cause aberrant cell-fate specification at the wing margin. This
81 disruption of patterning does not occur through general enhanced proliferation, but may
82 be due to misregulation of Myc target genes, including Chronologically inappropriate
83 morphogenesis (Chinmo). Hence, Brat acts as an important growth regulator and
84 protective factor during regeneration, by constraining levels of Myc, Chinmo, and
85 possibly other Myc targets to prevent errors in patterning, cell-fate specification, and
86 differentiation in the regenerating tissue.

87

Results

Brat suppresses regenerative growth and is required for wing margin cell-fate specification during regeneration

To identify genes important for regenerative growth and re-patterning, we performed a candidate screen, using our wing imaginal disc ablation system (23). The primordial wing was targeted for ablation at the early third-instar larval stage by using *rotund-GAL4* to drive the expression of the proapoptotic gene *reaper* for 24 hours (Figure 1A). Our ability to restrict damage to 24 hours was provided by *tubulin-GAL80^{ts}*, which can inhibit GAL4 activity at 18°C, but allows GAL4-driven cell death at 30°C in the 24-hour window. The extent of wing imaginal disc regeneration in the larvae was reflected in the adult wing size. Hence, the resulting adult wings were scored based on size and patterning features to identify mutants that affect genes that are involved in regulating regenerative growth and establishment of cell fates. There is inherent variability in this system because of its sensitivity to environmental conditions such as temperature, humidity, and food quality, causing the results of different experiments to vary slightly (14,48–51). Animals with the same genotype within an experiment also showed some variation, due to stochastic differences in the time each animal takes to eclose, with animals that take longer to eclose having larger wings (23,50). However, differences between control and mutant animals using this system are reproducible, consistent, and have identified key regeneration genes (32,49–51).

109 Using this genetic ablation system, we identified the gene *brain tumor (brat)* as an
110 important regulator of regenerative growth. *brat*^{1}/+ mutants that did not experience
111 damage during development had adult wings that were not significantly different in size
112 from controls (Figure S1A). However, after ablation and regeneration were induced,
113 *brat*^{1}/+ mutants showed enhanced regeneration and had adult wings that were, on
114 average, much larger than controls that had also undergone regeneration (Figure 1B
115 and 1C). We confirmed this enhanced regeneration phenotype in heterozygotes for
116 three other *brat* mutant alleles: *brat*^{192}, *brat*^{150} (52) and *brat*^{11} (53)(Figure S1B).

117

118 Interestingly, we also discovered a role for *brat* in cell-fate specification during
119 regeneration. After normal development, *brat*^{1}/+ mutants had adult wings that were
120 patterned normally (Figure 1D-E and Figure S1C). To confirm that reduction in *brat*
121 expression does not cause patterning errors during normal development, we knocked
122 down Brat levels in the entire wing pouch using *brat* RNAi, which resulted in adult wings
123 that were patterned normally (Figure S1D and S1E). A previous study in which Brat
124 levels were reduced in the anterior and posterior compartments of the wing also did not
125 report any patterning defects (54). However, when discs were ablated and allowed to
126 regenerate, *brat* heterozygous mutant wings showed aberrant patterning such that the
127 wing margin lost sensory bristles and vein material (Figure 1F and 1G). By contrast,
128 control regenerated wings lost margin tissue at a lower frequency (Figure 1H and 1I).
129 Furthermore, the extent of margin tissue lost was not as severe in control regenerated
130 wings as compared to *brat*^{1}/+ regenerated wings (Figure 1H and 1I). Similar to the

131 enhanced regeneration seen in *brat* mutants, we confirmed the loss-of-margin defect in
132 heterozygotes for the additional three mutant alleles (Figure S1F).

133

134 ***brat* regulates entry into metamorphosis**

135 Tissue damage in imaginal discs can induce a systemic response in the larvae, which
136 extends the larval phase of development and delays pupariation (23,55). This delay in
137 pupariation is due to expression of the relaxin-like peptide *ilp8* in damaged discs
138 (56,57). To determine whether *brat* mutants regenerated better due to an enhanced
139 delay in pupariation, we measured rates of pupariation in control and mutant animals.
140 We found that during normal development, control and $brat^{1}$/+ animals pupariated at the
141 same time, indicating that the two genotypes develop at similar rates (Figure S2A). After
142 disc damage, *brat* mutants delayed pupariation an additional day compared to controls
143 in which discs were also damaged (Figure 2A and Figure S2B). Note that direct
144 comparisons cannot be made between regenerating larvae that spent 24 hours at 30°C
145 (Figure 2A, Figure S2B) and normally developing larvae that remain at 18°C (Figure
146 S2A), due to the effects of temperature on development. Our data show that *brat*/+
147 mutants are able to stay in the larval stage even longer than controls, giving them more
148 time to regenerate.

149

150 To determine why discs with reduced Brat had an increased delay in pupariation, we
151 measured *ilp8* transcript levels through qPCR. Undamaged control animals express
152 very low *ilp8* levels. However, after regeneration was induced, we saw an 80-fold

153 increase in *ilp8* levels in controls, while the *brat*^{1}/+ animals showed a 140-fold increase
154 (Figure 2B). Thus, *brat* suppresses *ilp8* during regeneration, regulating the timing of
155 pupariation.

156

157 ***brat* restricts growth and proliferation during regeneration**

158 Regenerative growth occurs through localized cell proliferation at the wound site
159 (23,58).The proliferating cells, known as the blastema, give rise to the regenerated
160 tissue. The blastema and the subsequent regenerated wing pouch can be labeled with
161 the wing primordium marker Nubbin (Nub) (59). To determine whether *brat*^{1}/+ discs
162 regenerated better due to increased growth rates in the wing pouch, we measured the
163 area of the Nub-expressing cells in control and *brat*^{1}/+ regenerating discs. In the initial
164 stages of regeneration, the control and mutant had similar Nub-expressing areas,
165 indicating equal ablation and equal early regrowth. However, by 48 hours after tissue
166 damage (recovery time 48, or R48), *brat*^{1}/+ wing discs had a significantly bigger Nub-
167 expressing pouch than the control (Figure 2D-F), indicating that *brat/*+ mutants were
168 regenerating faster than controls. To assess whether this difference in growth rates was
169 due to differences in proliferation, we counted cells going through mitosis by quantifying
170 Phospho-histone H3 (PH3)-positive nuclei in the regenerating blastema. Reduction of
171 *brat* resulted in a significantly higher number of PH3-positive nuclei per area at R0, but
172 this increased proliferation had subsided to normal levels by R24 (Figure 2G-I). To
173 confirm that the increased number of PH3-positive nuclei were not simply due to an
174 increased number of total cells in the blastema, we also counted total Nubbin-positive

175 nuclei in the regenerating blastema to calculate a ratio of proliferating cells to blastema
176 cells (Figure S2C). These data confirm increased proliferation in *brat*^{1}/+ regenerating
177 discs at R0. Differences in proliferation early in regeneration often become evident later
178 when measuring wing pouch area (51). Therefore, reduction of *brat* gives the
179 regenerating tissue a growth advantage early in regeneration, resulting in a measurable
180 difference in tissue area by R48.

181

182 Wingless (Wg) and Myc are regulators of regenerative growth and are upregulated at
183 the wound site after damage (20,21,23). Interestingly, Brat regulates stem cell
184 differentiation in the brain by suppressing self-renewal signaling pathways such as Wnt
185 signaling, and acting as a post-transcriptional inhibitor of Myc, to enable specification of
186 progenitor cell fate (42,60). Additionally, Brat overexpression can suppress Myc at the
187 post-transcriptional level in wing disc epithelial cells, although loss of *brat* does not lead
188 to elevated Myc protein in wing discs during normal development (54). To determine
189 whether these regulators of regenerative growth are upregulated in *brat*^{1}/+ regenerating
190 discs, we examined the expression of Wg and Myc. Wg is normally expressed along the
191 Dorso-ventral (DV) boundary and in two concentric circles at the inner and outer edge of
192 the wing pouch (61) (Figure 3A), and Myc is expressed in the wing pouch, but is
193 repressed in the cells at the DV boundary as they undergo cell cycle and growth arrest
194 (62) (Figure 3B). Both Wg and Myc expression were comparable to controls in
195 undamaged *brat*^{1}/+ discs (Figure S3A-E). When damage is induced, Wg is upregulated
196 throughout the blastema by R0 (23) (Figure 3C). Reduction of *brat* expression resulted
197 in significantly higher levels of Wg expression at R0 (Figure 3D and 3E) but not at R24

198 (Figure 3F). After ablation, Myc expression is elevated in the regenerating tissue (23)
199 (Figure 3G and 3H). *brat*^{1}/+ discs showed significantly higher levels of Myc at R0, which
200 were sustained through R24 (Figure 3I-K). Thus, being heterozygous mutant for *brat*
201 caused an increase in the levels of both Wg and Myc early in regeneration. The
202 elevated expression of these growth regulators likely explains the high proliferation seen
203 in *brat*^{1}/+ discs at R0, and the larger wing pouch at R48.

204

205 ***brat* is required for margin cell-fate specification during regeneration**

206 Reduction of *brat* during regeneration caused patterning defects specifically at the wing
207 margin, resulting in the loss of vein at the margin and loss of sensory bristles (Figure
208 1G). Thus, *brat* is required for correct cell-fate specification at the DV boundary during
209 regeneration. The wing imaginal disc is divided into the dorsal and the ventral
210 compartments, with expression of the LIM-homeodomain protein Apterous (Ap) in
211 dorsal cells. The juxtaposition of the dorsal and ventral cells forms the DV boundary,
212 which develops into the adult wing margin (63) (Figure 4A). Notch (N) and Wg signaling
213 at the DV boundary are crucial for the correct organization and cell-fate specification at
214 the boundary (64). *cut (ct)* and *achaete (ac)* are margin-specific genes that are
215 expressed downstream of N and Wg signaling. *ct* is required for the specification of the
216 wing margin, and *ac* specifies the pro-neural sensory organ precursors (64,65) (Figure
217 4A).

218

219 To investigate whether the errors in fate specification seen in *brat*^{1}/+ discs were due to
220 a compromised compartment boundary, we examined the expression of Ap using the
221 *ap-lacZ* reporter. *ap-lacZ* expression showed a clear DV boundary in the undamaged
222 control discs (Figure 4B). The DV boundary remained intact after ablation in control and
223 *brat*^{1}/+ discs (Figure 4C-D, Figure S4A and S4B). *ap-lacZ* expression was also seen in
224 the debris found in the damaged wing imaginal disc, due to the perdurance of β-gal. Wg
225 expression was restored to its normal DV expression by R48 in both control and *brat*^{1}/+
226 discs (Figure S4C and S4D). Therefore, the patterning defects were not caused by
227 disruptions in the DV boundary or changes in Wg expression.

228

229 Next, we examined N signaling in *brat*^{1}/+ discs due to its critical role in specifying fates
230 at the DV boundary. We used a N signaling reporter, which uses *Notch Response*
231 *Elements* (*NREs*) that bind to the Notch co-receptor Suppressor of Hairless, to drive the
232 expression of GFP (66). No difference was detected in the expression of the N reporter
233 for undamaged control and *brat*^{1}/+ discs (Figure 4E and 4F). N signaling at the DV
234 boundary was restored by R24 in controls and continued at R48 (Figure 4G and 4H).
235 Note that the reporter signal can also be seen in cellular debris in the regenerating discs
236 due to the perdurance of GFP. Interestingly, *brat*^{1}/+ discs showed highly elevated levels
237 of the N signaling reporter at both these time points (Figure 4I and 4J). This result is
238 consistent with recent evidence demonstrating Brat's ability to attenuate N nuclear
239 transport in the brain (67). We wondered whether this elevated N signaling could also
240 disrupt margin fates. However, overexpressing the N-intracellular domain in the wing
241 pouch during the 24-hour ablation period (Figure S4E and S4F) resulted in adult wings

242 that were patterned remarkably well, with significantly fewer wings showing any margin
243 defects when compared to the control (Figure S4G). Thus, increased N activity during
244 regeneration suppresses margin defects. Additionally, decreasing N signaling activity in
245 *brat*^{1}/+ regenerating discs by using a mutation in the *anterior pharynx defective 1 (aph-*
246 *1)* gene was unable to rescue the *brat* heterozygous phenotype. *aph-1*^{D35}/+ discs
247 showed significantly reduced N signaling during normal development (Figure S4H-J)
248 and at R24 during regeneration (Figure S4K-M), but could not rescue the loss of margin
249 phenotype in the *brat* mutant (Figure S4N). Thus, while Brat constrains N signaling
250 during regeneration, the elevated N signaling in *brat*^{1}/+ mutants does not cause the
251 margin cell-fate specification defects.

252

253 To determine whether the loss of margin cell fates was due to apoptosis of those cells
254 later in regeneration, we immunostained regenerating discs for the cleaved caspase
255 Dcp-1 as a marker of cell death, and Wg to mark the margin. We did not observe dying
256 cells in the margin in either control or *brat*^{1}/+ regenerating discs (Figure S4 C-D).

257

258 ***brat* specifies margin fate by controlling the expression of Cut and Achaete**

259 To understand how patterning was disrupted in *brat*^{1}/+ regenerating discs, we examined
260 expression of margin cell-fate genes. Cut (Ct) expression was present along the DV
261 boundary in both undamaged control and *brat*^{1}/+ discs (Figure 4K and 4L), consistent
262 with our results showing that adult undamaged *brat*^{1}/+ wings do not have margin
263 defects (Figure S1D). In control regenerating discs, Ct expression was detected at the

264 DV boundary at R72, which is when regeneration and repatterning are largely complete
265 (Figure 4M). By contrast, Ct expression was either not observed in *brat*^{1}/+ discs or was
266 still missing in segments of the DV boundary at R72 (Figure 4N and 4O). These results
267 indicate a specific error in cell-fate specification, as the DV boundary was intact at R72
268 (Figure S4A and S4B). Undamaged control and *brat*^{1}/+ discs also showed appropriate
269 Ac expression in two stripes of cells directly flanking the DV boundary in the anterior
270 half of the disc (Figure 4P and 4Q). Ac expression was also detected in control
271 regenerating discs at R72 (Figure 4R). While Ac-expressing cells appeared in *brat*^{1}/+
272 discs, they were not clearly separated across the DV boundary (Figure 4S). This finding
273 is consistent with previous reports showing that Ct suppresses Ac at the margin, and
274 mutations in *ct* lead to aberrant expression of Ac at the DV boundary, followed by
275 degeneration of the wing margin through cell death (68,69).

276

277 **High Myc expression perturbs margin cell-fate specification during regeneration**

278 Our results show that Brat both restricts regenerative growth and ensures correct cell-
279 fate specification at the wing margin. Interestingly, JNK signaling in regenerating tissue
280 can cause aberrant posterior-to-anterior cell-fate changes, which can be suppressed by
281 a regeneration-specific protective factor, Taranis, to ensure correct patterning of the
282 regenerating tissue (32). Therefore, we wondered whether unconstrained regenerative
283 growth, or unconstrained expression of growth drivers, could also have deleterious side
284 effects such as loss of margin cell fates. As Wg expression is normal during late
285 regeneration and we have ruled out elevated N signaling as the causative factor for the

286 cell-fate errors that occurred in *brat*^{1}/+ regenerating discs, we wondered whether high
287 Myc levels caused by reduced Brat could cause the margin defects.

288

289 Brat overexpression can suppress Myc in wing imaginal disc cells (54), and in
290 undamaged wing discs Brat protein levels were elevated at the DV boundary where Myc
291 was reduced (Figure 5A and 5A'), suggesting that Brat may regulate Myc at the DV
292 boundary. Furthermore, our results showed that regenerating *brat/*+ mutant discs
293 experienced elevated Myc levels compared to controls (Figure 3G-K). Previous studies
294 demonstrated that Brat regulates Myc at the post-transcriptional level (54). To confirm
295 that Brat is also regulating *myc* post-transcriptionally during regeneration, we measured
296 *myc* transcript levels through qPCR. Regenerating discs showed significantly increased
297 transcription of *myc* compared to undamaged controls. However, there was no
298 significant difference in *myc* transcript levels between regenerating control and *brat*^{1}/+
299 discs at R0 and R24 (Figure 5B and 5C), indicating that Brat's regulation of Myc must
300 be post-transcriptional.

301

302 To test whether the elevated Myc protein levels could cause margin defects during
303 regeneration and phenocopy the *brat* mutation, we overexpressed Myc in the wing
304 pouch during the 24-hour ablation period. Myc was highly upregulated at R0 (Figure 5D-
305 F), but Myc levels had returned to normal by R24 (Figure 5F). Overexpression of Myc
306 also resulted in a significantly higher number of proliferating nuclei in the regenerating
307 tissue at R0, similar to *brat*^{1}/+ discs (Figure 5G-I). Remarkably, we observed that adult

308 wings resulting from Myc-overexpressing regenerating discs also showed margin
309 defects similar to the *brat*^{1}/+ wings (Figure 5J and 5K). Moreover, the frequency of
310 margin defects in the adult wings resulting from Myc-overexpressing regenerating discs
311 was even higher than in adult wings resulting from *brat*^{1}/+ regenerating discs (Figure
312 5L). This difference in severity of phenotype correlates with levels of Myc at R0; in
313 *brat*^{1}/+ regenerating discs Myc levels are higher than the control by 1.4 and 1.5-fold at
314 R0 and R24 respectively (Figure 3K), and in Myc-overexpressing regenerating discs,
315 Myc levels are higher than control by 2.75 fold at R0 but become similar to controls by
316 R24 (Figure 5F). Thus, elevated levels of Myc alone can cause errors in margin cell-fate
317 specification. Similar to *brat*^{1}/+ discs, *ap-lacZ* expression showed that the compartment
318 boundary was not compromised in Myc-overexpressing regenerating discs (Figure 5M
319 and 5N). Likewise, Ct expression was missing in segments at the DV boundary as in the
320 *brat*^{1}/+ discs (Figure 5O and 5P).

321

322 Overexpressing Myc for a 24-hour window during normal development resulted in 3
323 adult wings out of 730 that showed any margin defects (Figure S5A). Even in these
324 wings, only one segment of the margin was affected. To rule out the possibility that
325 transient overexpression of Myc during development may not be sufficient to perturb
326 patterning, we overexpressed Myc continuously after the animals entered the third
327 instar larval stage. Continuous Myc overexpression proved to be lethal for many
328 animals. While the flies that survived had significantly smaller wings, the margins
329 showed no defect (Figure 5Q and 5R). 31 hours of Myc overexpression during normal
330 development showed significantly higher Myc protein levels (Figure 5S-U) but did not

331 interfere with Ct expression (Figure 5V and 5W). These data indicate that high Myc
332 levels do not cause cell-fate specification errors during normal development, and the
333 extensive loss of wing margin induced by high Myc expression is a regeneration-specific
334 phenotype.

335

336 **Loss of Myc expression also perturbs margin cell-fate specification during**
337 **regeneration**

338 We hypothesized that if the *brat* phenotype was due to elevated Myc levels, we would
339 be able to rescue the phenotype by reducing Myc levels in the *brat* mutant. For this
340 purpose, we used dm^4, which is a null allele of Myc (70). Surprisingly, we observed that
341 the dm^4/+ mutants alone showed margin defects in the regenerated wings at a
342 frequency similar to $brat^1$/+, even though the dm^4/+; $brat^1$/+ double mutant showed
343 slightly reduced frequency of margin defects (Figure S5B). To confirm that Myc levels
344 were reduced in the dm^4/+ mutants, we quantified Myc protein through immunostaining.
345 We observed that there was no significant difference in Myc expression levels between
346 the dm^4/+ mutant and control, both during development and regeneration (Figure S5C
347 and S5D). Indeed, Myc levels were trending higher in the dm^4/+ discs during
348 regeneration, perhaps accounting for the margin defects. The failure of the dm^4
349 mutation to reduce Myc levels could be due to compensatory expression of the
350 functional copy of the Myc locus. We next tried reducing Myc levels though RNAi.
351 Despite the RNAi expression being transient in our system, and only occurring in cells
352 that survive ablation, RNAi-mediated persistent knockdown has worked for multiple

353 genes, likely due to the shadow RNAi effect (71). Two RNAi lines could significantly
354 reduce Myc levels during normal development when expressed during early third instar
355 (Figure S5E). However, when Myc RNAi was expressed during the 24-hour ablation
356 period, Myc levels were not reduced at either R0 or R24, with one Myc RNAi line
357 showing significantly higher levels of Myc compared to the control (Figure S5F).

358

359 To reduce Myc levels without the possibility of compensatory expression from an
360 endogenous allele, we turned to the viable hypomorphic allele Myc^{P0}, which is reported
361 to eliminate Myc mRNA in the wing pouch (72). Indeed, we found that male larvae
362 hemizygous for Myc^{P0} did not show the typical Myc expression in third-instar wing discs,
363 and lacked upregulation of Myc during regeneration (Fig S5 G-H). The Myc^{P0} males
364 developed more slowly than control larvae, so we adjusted the timing of induction of
365 ablation later by 4 hours to coincide with the early third instar larval phase. Surprisingly,
366 we found that Myc^{P0} males that had undergone ablation and regeneration in the wing
367 discs also had adult wings that were missing substantial sections of their margins, as
368 did Myc^{P0}; $brat^{1}$/+ double mutants (Fig S5I). Indeed, immunostaining Myc^{P0} regenerating
369 discs showed gaps in *cut* expression, indicating disruption of margin fate (Fig S5J-K).
370 Therefore, reduction of Myc as well as elevation of Myc disrupts margin cell fate during
371 regeneration, underscoring the importance of tightly regulating expression of this pro-
372 regeneration, pro-growth factor. However, this phenotype means that rescuing the
373 $brat^{1}$/+ phenotype by reducing Myc is not possible, given that reducing Myc alone
374 disrupts the wing margin, and we cannot rule out the possibility that other Brat targets in
375 addition to Myc contribute to the patterning defects in $brat^{1}$/+ regenerated wings.

376 Importantly, animals that overexpressed Myc in the wing pouch during ablation did not
377 undergo a regeneration-induced pupariation delay (Figure S5L), confirming that Brat
378 regulates the entry into metamorphosis independently of its regulation of Myc.
379 Therefore, not all effects of reduced Brat are mediated through Myc.

380

381 **Enhanced proliferation does not disrupt margin cell-fate specification during**
382 **regeneration**

383 Myc is an important driver of regenerative growth, and yet, we found that cell-fate
384 specification during regeneration can be negatively affected if Myc levels are not
385 constrained. To test whether the aberrant patterning was a specific result of high Myc
386 levels or whether increases in growth and proliferation could, in general, cause margin
387 defects, we also increased proliferation during regeneration by overexpressing both
388 *cyclinE (cycE)* and *string (stg)*.

389

390 Overexpressing the cell cycle genes in the wing imaginal disc during the 24-hour
391 ablation period caused the resulting adult wings to be much larger than controls that
392 had also undergone damage and regeneration (Figure 6A), though not larger than a
393 normal wing. No significant regeneration-induced pupariation delay was seen, making
394 the enhanced regeneration even more remarkable (Figure 6B). Intriguingly, we did not
395 observe many margin defects for wings that had experienced *cycE* and *stg*
396 overexpression during regeneration (Figure 6C-E). Furthermore, we have not observed
397 this loss of margin phenotype with overexpression of other pro-regeneration genes such

398 as *dilp8* (data not shown). Thus, pattern disruption during regeneration appears to be
399 specifically associated with Myc overexpression and does not appear to be caused by
400 increased proliferation alone.

401

402 **Loss of cell-fate specification may be due to misregulation of Myc target genes**

403 Given that driving growth by overexpressing Cyclin E and String does not cause loss of
404 wing margin cell fates in regenerating tissue, this phenotype might be caused by
405 misregulation of one or more targets of the Myc transcription factor. To identify genes
406 that may regulate margin cell fate downstream of Myc, we screened through genes
407 reported in the literature as regulating *ct* expression, and identified one that was
408 misregulated in *brat*^{1}/+ and *UAS-Myc* regenerating discs. We have previously identified
409 the gene *Chronologically inappropriate morphogenesis (chinmo)* as a novel regulator of
410 regeneration (50). Chinmo is a transcription factor that regulates the balance between a
411 proliferative self-renewal state and a differentiated state in stem cells (73,74). Recent
412 work has shown that *chinmo* also maintains wing epithelial cells in an unspecified state
413 during development by inhibiting *ct* expression, and enhances regenerative potential
414 (75). Therefore, we included *chinmo* in our targeted screen for genes that are
415 misregulated in the *brat*^{1}/+ or *UAS-Myc* regenerating discs and that contribute to the
416 disruption of cell fate.

417

418 Several lines of evidence suggest that *chinmo* can be a transcriptional target of Myc.
419 First, the model organism Encyclopedia of Regulatory Networks (modERN) data show

420 Myc binding near the *chinmo* promoter (76). Second, ChIP-seq experiments in
421 *Drosophila* embryonic Kc cells have shown that Myc does indeed bind to the *chinmo*
422 locus (77). Finally, *chinmo* levels are upregulated in response to elevated Myc
423 expression in wing imaginal discs (78). To determine whether *chinmo* expression was
424 altered in $brat^1$/+ wing discs, we immunostained for Chinmo protein. Chinmo levels were
425 not significantly different in undamaged control and $brat^1$/+ discs (Figure 7A, 7B and
426 7E). However, Chinmo levels were significantly higher in $brat^1$/+ regenerating discs
427 compared to control regenerating discs at R24 (Figure 7C, 7D and 7F). To confirm
428 regulation of *chinmo* downstream of Myc, we examined Chinmo levels in regenerating
429 discs over-expressing Myc. Chinmo levels were elevated in Myc-overexpressing discs
430 at R0, when Myc overexpression was the highest (Figure 5F and Figure 7G-I).
431 However, Chinmo levels were restored to control levels by R24 in Myc-overexpressing
432 discs, consistent with the return of Myc levels to normal at this time point (Figure 5F and
433 Figure S6A-C). Interestingly, Myc and Chinmo expression almost perfectly co-localized,
434 consistent with the hypothesis that Myc regulates Chinmo expression (Figure S6A-B''').
435 Additionally, we observed a high correlation between Myc and Chinmo expression
436 levels in individual discs (Figure S6D and S6E). Undamaged discs overexpressing Myc
437 did not show elevated Chinmo levels (Figure S6F-H), possibly explaining why Myc
438 overexpression during normal development did not cause margin defects.

439

440 While *chinmo* mRNA can be a direct Brat target (39), *chinmo* is regulated at the level of
441 transcription in the wing imaginal disc (75). To confirm the absence of regulation of
442 *chinmo* mRNA by Brat during regeneration, we assessed expression of mCherry from a

443 transgene in which the *chinmo* UTRs were fused to the *mCherry* coding region to serve
444 as a reporter for *chinmo* mRNA regulation (*UAS-mCherry-chinmoUTR*) (79). We did not
445 detect any change in mCherry levels in *brat*^{1}/+ regenerating discs compared to control
446 regenerating discs, indicating that reduction of Brat does not impact the *chinmo* mRNA
447 reporter and Brat does not likely regulate *chinmo* mRNA in regenerating discs (Fig S6I).

448

449 Thus, the loss of *ct* expression and loss of margin cell fates in *brat/*+ regenerating discs
450 and *UAS-Myc* regenerating discs may be due, at least in part, to upregulation of Myc
451 targets, including *chinmo*. Importantly, other unidentified Myc targets likely also
452 contribute to *ct* misregulation in regenerating discs with reduced Brat or overexpressed
453 Myc. To test whether expression of *chinmo* in the regeneration blastema is sufficient to
454 disrupt the margin, we expressed *UAS-chinmo* alongside the ablation system. Doing so
455 led to a moderate level of gaps in cut expression in R72 regenerating discs (4/14
456 compared to 0/12 for controls) (Figure 7J, K). To test whether the loss of margin in
457 regenerating wing discs overexpressing Myc is due at least in part to expression of
458 *chinmo*, we asked whether the phenotype could be ameliorated by a *chinmo* mutation.
459 Indeed, regenerating wing discs overexpressing Myc but heterozygous for *chinmo*^{1} had
460 significantly less margin loss compared to those just overexpressing Myc (Figure 7L).
461 Thus, we have identified at least one Myc target that contributes to disruption of cell fate
462 in regenerating tissue with Myc expression elevated beyond what is normally found in
463 the regeneration blastema.

464

465 Based on our findings, we propose a model in which pro-growth factors are important
466 for coordinating regenerative growth, but can lead to deleterious side effects by
467 perturbing cell-fate gene expression and patterning. Brat prevents a prolonged
468 proliferative and unspecified state in regenerating wing discs by constraining Wg, Ilp8,
469 Myc, and Myc targets, to enable cessation of growth, induction of cell-fate specification,
470 and entry into metamorphosis (Figure 8).

471

472 **Discussion**

473 Here we have shown that Brat acts as a protective factor during regeneration, in part by
474 constraining levels of the transcription factor Myc, which promotes growth and
475 proliferation but also inhibits cell-fate specification. If Brat is unable to perform its
476 protective function during regeneration, Myc levels increase unchecked, resulting in
477 misregulation of its targets, causing loss of proper cell fates at the wing margin.

478

479 Myc is broadly used across organisms to promote proliferation and prevent
480 differentiation (80,81). It is is required for efficient regeneration, and increased levels
481 can enhance regeneration in both younger discs as well as mature discs that normally
482 regenerate poorly (23,25). Nevertheless, we have found that while these abnormally
483 high Myc levels can enhance regenerative growth, they can also perturb differentiation
484 by misregulating target genes such as Chinmo. Thus, enhanced regeneration happens
485 at the expense of correct cell-fate specification. Intriguingly, our attempts to rescue the
486 *brat/+* phenotype by reducing Myc led to the discovery that loss of Myc expression in

487 the regeneration blastema also leads to loss of margin cell fates. Many Myc targets are
488 ribosomal protein genes, and, interestingly, adults transheterozygous for mutations in
489 the ribosomal protein gene *RpL38* also have missing wing margins even without
490 damage and regeneration of the wing disc (82). This finding provides precedent for
491 disruption of margin fates when ribosomal protein expression is reduced, and suggests
492 that the reasons for the lost margin in the Myc^{P0} and *UAS-Myc* regenerating discs may
493 be different. Importantly, expression of *ct* and possibly other cell-fate genes requires an
494 appropriate amount of Myc, with too much or too little Myc disrupting cell fate. This
495 phenomenon of requiring just the right amount of signaling or gene activity is not
496 unprecedented, as we have previously shown that activation of JNK signaling after wing
497 disc damage requires the right amount of reactive oxygen species (ROS) production;
498 too much ROS and too little ROS both lead to inadequate JNK activity and poor
499 regeneration (51).

500

501 Brat promotes differentiation in *Drosophila* larval neuroblasts and ovarian germline stem
502 cells by asymmetrically segregating to one of the daughter cells where it post-
503 transcriptionally inhibits Myc (41,42). This daughter cell is then able to differentiate while
504 the other daughter cell remains a stem cell. In *brat* mutants, progeny of stem cells are
505 unable to differentiate, resulting in an abnormal expansion of the stem-cell population,
506 which can form tumors in the brain (40–43). Thus, Brat protects these tissues from
507 overproliferation of stem cells. Importantly, wing imaginal disc regeneration is not stem-
508 cell based, but in wing disc regeneration Brat also inhibits Myc to allow correct cell-fate
509 specification. Based on these similarities in function, Brat likely acts as a protective

510 factor across different biological contexts, including regeneration that does not employ
511 stem cells.

512

513 We have previously shown that JNK signaling can induce posterior-to-anterior fate
514 changes in regenerating wing discs, which can be prevented by the protective factor
515 Taranis (32). In addition, we have shown that the chromatin-remodeling SWI/SNF BAP
516 complex, defined by the complex-specific component Osa, similarly prevents aberrant
517 posterior-to-anterior fate changes in regenerating wing discs (83). We have now
518 identified a third protective factor, Brat, which is needed specifically for correct
519 patterning of the regenerating wing margin. Interestingly, while elevated JNK signaling
520 causes anterior markers to appear in the posterior wing compartment, it does not cause
521 margin loss, indicating that posterior fate and margin fate are regulated in distinct ways
522 (32). Protective factors such as Tara, Osa, and Brat are important for maintaining the
523 balance between fate specification and regenerative potential, but they do so by using
524 very different mechanisms. While the molecular function of Tara is unknown, genetic
525 interactions in *Drosophila* coupled with the demonstrated functions of its vertebrate
526 homologs suggest it may regulate gene expression at the level of transcription and
527 chromatin (84–87). By contrast, Brat acts as a translational repressor by negatively
528 regulating translation and stability of its target mRNAs (88,89). Tara is required to
529 prevent fate changes induced by JNK signaling, which is necessary for wound repair
530 and regeneration but is not required for the normal growth of the wing. By contrast, Myc
531 is required for both development and regeneration of the wing disc, but is constrained
532 by Brat only during regeneration.

533

534 An important open question in the field of regeneration is how patterning and cell-fate
535 specification are regulated in regenerating tissue, and whether these mechanisms are
536 different from the developmental program. Many studies have highlighted that
537 regeneration must be distinct from development in some ways, because the damaged
538 tissue already has complex patterning, and the wound-healing response causes strong
539 activation of signaling pathways, some of which are not normally present in developing
540 tissue (1,3,25,30–35). We are just beginning to identify regulators like Brat that are
541 crucial for attenuating regenerative growth signaling and shielding the regenerating
542 tissue from the harmful side effects of such signaling. Identification of these regulators
543 highlights the fact that the regenerating tissue is distinct from normally developing
544 tissue. Since regeneration signaling is complex and comprised of many signaling
545 pathways, additional factors that play protective roles during regeneration likely exist.
546 Identification of these factors will be important for the development of clinical therapies
547 targeted at tissue repair, enabling these therapies to protect against the deleterious side
548 effects of exogenous and unconstrained pro-growth signaling.

549

550 **Materials and Methods**

551 **Ablation and Regeneration experiments**

552 Ablation experiments were done as previously described (32). Briefly, cell death was
553 induced by driving *UAS-reaper* under *rotund-GAL4*, with *GAL80^{ts}* for temporal control.
554 Animals were raised at 18°C for 7 days after egg lay (AEL) (early third instar) before

555 they were shifted to a 30°C circulating water bath for 24 hours. Animals were brought
556 back to 18°C to allow regeneration. Wing discs were dissected at different time points
557 after the end of ablation, or the animals were allowed to grow to adulthood to observe
558 the adult wing phenotype. Undamaged control wing discs were the same genotype as
559 the experimental animals but kept at 18°C and dissected on day 9 after egg lay, which
560 is mid-late third instar. For undamaged adult wings, the animals were kept at 18°C until
561 after eclosion. Any other undamaged conditions used are mentioned specifically in the
562 figure legends.

563

564 **Fly stocks**

565 The following *Drosophila* stocks were used: w^{1118} (wild type)(90), w^{1118} *; rnGAL4, UAS-*
566 *rpr, tubGAL80ts/TM6B,tubGAL80* (23), $brat^{1}$ (91)(FBst0003988), $brat^{192}$ and $brat^{150}$
567 (52)(a gift from Juergen Knoblich, Austrain Academy of Science), $brat^{11}$ (53)(a gift from
568 Chen-Yu Lee, University of Michigan), *Df(2L)Exel8040* (92)(FBst0007847),
569 *Df(2L)TE37C-7* (93)(FBst0006089), *rnGAL4, tubGAL80ts/TM6B* (23),
570 *P{Trip.HM05078}attP2* (called *bratRNAi* in the text)(FBst0028590), *P{CaryP}attP2*
571 (called *attP2* control in the text)(FBst0036303), *{PZ}*ap^{rK568} (94)(FBst0005374), *NRE-*
572 *GFP* (66)(FBst0030727), *UAS-Nintra* (a gift from Gary Struhl, Columbia University),
573 $aph\text{-}1^{D35}$ (95)(FBst0063242), *UAS-Myc* (72)(FBst0009674), *UAS-cycE, stg* (a gift from
574 Laura Buttitta, University of Michigan), dm^{4} (70), *P{GD1419}v2947* (called *MycRNAi#1*
575 in the text)(VDRC ID# 2947) and *P{GD1419}v2948* (called *MycRNAi#2* in the
576 text)(VDRC ID# 2948), *P{GD6000}v15293* (called control in the text) (VDRC ID#

577 15293), *Myc*^{P0} (72) (FBal0100372), UAS-mCherry^{chinmoUTRs} (73).All fly stocks are
578 available from the Bloomington Drosophila Stock Center unless stated otherwise.

579

580 **Pupariation timing**

581 Pupariation experiments were performed in a similar manner to the ablation
582 experiments. Starting at day 9, newly formed pupal cases were counted in each vial.
583 Pupal cases were counted every 24 hours, up until day 15. Pupariation rates from three
584 independent experiments were used to calculate the average plotted in the graphs.

585

586 **Immunohistochemistry**

587 Immunostaining was carried out as previously described (23). Primary antibodies were
588 rat anti-Brat (1:200) (37) (a gift from Robin Wharton, Ohio State University), mouse anti-
589 Nubbin (1:500) (96) (a gift from Steve Cohen, University of Copenhagen), rabbit anti-
590 Phospho-Histone H3 (1:500) (Millipore), mouse anti-Wingless (1:100) (The
591 Developmental Studies Hybridoma Bank [DSHB]), rabbit anti-dMyc (1:500 or 1:250)
592 (Santa Cruz Biotechnologies), mouse anti-βgal (1:100) (DSHB), mouse anti-Cut (1:100)
593 (DSHB), mouse anti-Achaete (1:10)(DSHB), rat anti-Chinmo (1:500) (a gift from Nick
594 Sokol, Indiana University), and anti-cleaved Dcp-1 (1:250)(Cell Signaling #9578). The
595 Developmental Studies Hybridoma Bank (DSHB) was created by the NICHD of the NIH
596 and is maintained at the University of Iowa, Department of Biology, Iowa City, IA 52242.
597

598 Secondary antibodies were AlexaFluor probes (1:1000) (Life Technologies). DNA was
599 marked using TO-PRO3 (1:500) (Life Technologies) or DAPI (1:5000 of 0.5 mg/mL
600 stock) (Sigma). Discs were mounted in Vectashield mounting medium (Vector
601 Laboratories).
602
603 Discs were imaged on a Zeiss LSM 510 or a Zeiss LSM 700 confocal microscope.
604 Parameters for imaging were identical for quantified images. Images were processed
605 using ZEN lite (Zeiss), ImageJ (NIH) and Photoshop (Adobe). Maximum intensity
606 projections were created for the confocal images. Fluorescence intensity was measured
607 within the wing pouch as marked by anti-Nubbin or by using the morphology of the
608 undamaged wing disc. Myc and Chinmo intensities were measured by outlining the
609 region expressing elevated Myc or Chinmo levels. *NRE-GFP* intensity was measured by
610 outlining the GFP-expressing region at the DV boundary.
611
612 **Adult wing quantifications**
613 Adult wings were mounted in Gary's Magic Mount (Canada balsam [Sigma] dissolved in
614 methyl salicylate [Sigma]). Images were taken with an Olympus SZX10 microscope with
615 an Olympus DP21 camera using the CellSens Dimension software (Olympus).
616
617 All adult wings that were 75% or 100% the size of a normal wing were used to quantify
618 the loss of the wing margin. The wing margin was divided into five segments defined by
619 where the wing veins intersect the margin. Each wing was scored for the number of
620 segments with missing margin to assess the extent of the patterning defect.

621 Percentages from the three independent experiments were used to calculate averages
622 plotted in the graphs. The area of undamaged and regenerated wings was measured
623 using ImageJ (NIH). ImageJ was also used to measure the percentage of linear length
624 of margin lost for the entire perimeter of the wing. Graphs were plotted using Excel and
625 Graphpad Prism 7.
626

627 **qPCR**

628 For quantitative PCR (qPCR), 40-60 wing imaginal discs were collected in Schneider's
629 medium and stored at -80°C. RNA was extracted using the Qiagen RNeasy Mini Kit
630 (#74104), and cDNA synthesis was performed using the Superscript III First Strand
631 Synthesis kit (#11752-050). qPCR reactions using the Power SYBR Green MasterMix
632 (ABI) were run on the ABI Step One Plus Real Time PCR System. The experiment
633 consisted of 3 biological replicates. For each biological replicate there were three
634 technical replicates. Gene expression was analyzed by the $\Delta\Delta C_t$ method and
635 normalized to *Gapdh2* expression. The following primers were used: *Gapdh2* forward
636 primer (GTGAAGCTGATCTCTTGGTACGAC), *Gapdh2* reverse primer
637 (CCGCGCCCTAATCTTTAACTTTTAC) (97), *ilp8* primers used from Qiagen
638 (QT00510552), *dmyc* forward primer (AACGATATGGTGGACGATGG), and *dmyc*
639 reverse primer (CGGCAGATTGAAGTTATTGTAGC) (98). For qPCR experiments
640 undamaged controls were *rnGAL4, tubGAL80ts/TM6B* females crossed to w^{1118} males
641 and shifted to 30˚C for 24 hours at 7 days AEL. Discs were dissected either immediately
642 or 24 hours after shifting the animals back to 18˚C for R0 and R24 time points,
643 respectively.

Acknowledgements

The authors would like to thank Amanda Brock and Sumbul Khan for critical reading of the manuscript and helpful discussions. We also thank Juergen Knoblich, Cheng-Yu Lee, Gary Struhl, Robin Wharton, Nick Sokol, Laura Buttitta, and Cedric Maurange for reagents. Stocks obtained from the Bloomington Drosophila Stock Center (NIH P40OD018537) were used in this study. Transgenic fly stocks were obtained from the Vienna Drosophila Resource Center (VDRC, www.vdrc.at). Antibiodies were obtained from the Developmental Studies Hybridoma Bank, created by the NICHD of the NIH and maintained at The University of Iowa, Department of Biology, Iowa City, IA 52242.

Author Contribution Section

Experiments were designed by SNFA and RKSB, and conducted and analyzed by SNFA and FT-YH. The manuscript was written by SNFA and RKSB.

Competing interests

The authors declare no competing interests.

Data Availability

All relevant data are available at (insert web address for UIUC library repository when manuscript accepted) and upon request.

665 **References**

666

667 1. Bosch M, Serras F, Martín-Blanco E, Baguñà J. JNK signaling pathway required for
668 wound healing in regenerating Drosophila wing imaginal discs. Dev Biol.
669 2005;280(1):73–86.

670 2. Bergantiños C, Corominas M, Serras F. Cell death-induced regeneration in wing
671 imaginal discs requires JNK signalling. Development. 2010;137(7):1169–79.

672 3. Bosch M, Bishop SA, Baguña J, Couso JP. Leg regeneration in Drosophila abridges
673 the normal developmental program. Int J Dev Biol. 2010;54(8–9):1241–50.

674 4. Tasaki J, Shibata N, Sakurai T, Agata K, Umesono Y. Role of c-Jun N-terminal
675 kinase activation in blastema formation during planarian regeneration. Dev Growth
676 Differ. 2011;53(3):389–400.

677 5. Martín R, Pinal N, Morata G. Distinct regenerative potential of trunk and appendages
678 of Drosophila mediated by JNK signalling. Development. 2017;144(21):dev.155507.

679 6. Bando T, Ishimaru Y, Kida T, Hamada Y, Matsuoka Y, Nakamura T, et al. Analysis of
680 RNA-Seq data reveals involvement of JAK/STAT signalling during leg regeneration in
681 the cricket Gryllus bimaculatus. Development. 2013;140(5):959–64.

682 7. Katsuyama T, Comoglio F, Seimiya M, Cabuy E, Paro R. During Drosophila disc
683 regeneration, JAK/STAT coordinates cell proliferation with Dilp8-mediated
684 developmental delay. Proc National Acad Sci. 2015;112(18):E2327–36.

685 8. Verghese S, Su TT. STAT, Wingless, and Nurf-38 determine the accuracy of
686 regeneration after radiation damage in Drosophila. Plos Genet. 2017;13(10):e1007055.

687 9. Nakamura T, Mito T, Bando T, Ohuchi H, Noji S. Molecular and Cellular Basis of
688 Regeneration and Tissue Repair. Cell Mol Life Sci. 2007;65(1):64.

689 10. Jiang H, Grenley MO, Bravo MJ, Blumhagen RZ, Edgar BA. EGFR/Ras/MAPK
690 Signaling Mediates Adult Midgut Epithelial Homeostasis and Regeneration in
691 Drosophila. Cell Stem Cell. 2011;8(1):84–95.

692 11. Fan Y, Wang S, Hernandez J, Yenigun VB, Hertlein G, Fogarty CE, et al. Genetic
693 Models of Apoptosis-Induced Proliferation Decipher Activation of JNK and Identify a
694 Requirement of EGFR Signaling for Tissue Regenerative Responses in Drosophila.
695 Plos Genet. 2014;10(1):e1004131.

696 12. Jin Y, Ha N, Forés M, Xiang J, Gläßer C, Maldera J, et al. EGFR/Ras Signaling
697 Controls Drosophila Intestinal Stem Cell Proliferation via Capicua-Regulated Genes.
698 Plos Genet. 2015;11(12):e1005634.

699 13. Bando T, Mito T, Maeda Y, Nakamura T, Ito F, Watanabe T, et al. Regulation of leg
700 size and shape by the Dachsous/Fat signalling pathway during regeneration.
701 Development. 2009;136(13):2235–45.

702 14. Sun G, Irvine KD. Regulation of Hippo signaling by Jun kinase signaling during
703 compensatory cell proliferation and regeneration, and in neoplastic tumors. Dev Biol.
704 2011;350(1):139–51.

705 15. Grusche FA, Degoutin JL, Richardson HE, Harvey KF. The Salvador/Warts/Hippo
706 pathway controls regenerative tissue growth in Drosophila melanogaster. Dev Biol.
707 2011;350(2):255–66.

708 16. Hayashi S, Ochi H, Ogino H, Kawasumi A, Kamei Y, Tamura K, et al.
709 Transcriptional regulators in the Hippo signaling pathway control organ growth in
710 Xenopus tadpole tail regeneration. Dev Biol. 2014;396(1):31–41.

711 17. Grijalva JL, Huizenga M, Mueller K, Rodriguez S, Brazzo J, Camargo F, et al.
712 Dynamic alterations in Hippo signaling pathway and YAP activation during liver
713 regeneration. Am J Physiol-gastr L. 2014;307(2):G196–204.

714 18. Hobmayer B, Rentzsch F, Kuhn K, Happel CM, Laue CC von, Snyder P, et al. WNT
715 signalling molecules act in axis formation in the diploblastic metazoan Hydra. Nature.
716 2000;407(6801):186.

717 19. Kawakami Y, Esteban CR, Raya M, Kawakami H, Martí M, Dubova I, et al. Wnt/β-
718 catenin signaling regulates vertebrate limb regeneration. Gene Dev. 2006;20(23):3232–
719 7.

720 20. McClure KD, Schubiger G. A screen for genes that function in leg disc regeneration
721 in Drosophila melanogaster. Mech Develop. 2008;125(1–2):67–80.

722 21. Schubiger M, Sustar A, Schubiger G. Regeneration and transdetermination: The
723 role of wingless and its regulation. Dev Biol. 2010;347(2):315–24.

724 22. Wehner D, Cizelsky W, Vasudevaro MD, Özhan G, Haase C, Kagermeier-Schenk
725 B, et al. Wnt/β-Catenin Signaling Defines Organizing Centers that Orchestrate Growth
726 and Differentiation of the Regenerating Zebrafish Caudal Fin. Cell Reports.
727 2014;6(3):467–81.

728 23. Smith-Bolton RK, Worley MI, Kanda H, Hariharan IK. Regenerative Growth in
729 Drosophila Imaginal Discs Is Regulated by Wingless and Myc. Dev Cell.
730 2009;16(6):797–809.

731 24. Hanovice NJ, Leach LL, Slater K, Gabriel AE, Romanovicz D, Shao E, et al.
732 Regeneration of the zebrafish retinal pigment epithelium after widespread genetic
733 ablation. Plos Genet. 2019;15(1):e1007939.

734 25. Harris RE, Setiawan L, Saul J, Hariharan IK. Localized epigenetic silencing of a
735 damage-activated WNT enhancer limits regeneration in mature Drosophila imaginal
736 discs. Elife. 2016;5:e11588.

737 26. Muneoka K, Bryant SV. Evidence that patterning mechanisms in developing and
738 regenerating limbs are the same. Nature. 1982;298(5872):298369a0.

739 27. Gupta V, Gemberling M, Karra R, Rosenfeld GE, Evans T, Poss KD. An Injury-
740 Responsive Gata4 Program Shapes the Zebrafish Cardiac Ventricle. Curr Biol.
741 2013;23(13):1221–7.

742 28. Roensch K, Tazaki A, Chara O, Tanaka EM. Progressive Specification Rather than
743 Intercalation of Segments During Limb Regeneration. Science. 2013;342(6164):1375–9.

744 29. Mader MM, Cameron DA. Photoreceptor Differentiation during Retinal Development,
745 Growth, and Regeneration in a Metamorphic Vertebrate. J Neurosci.
746 2004;24(50):11463–72.

747 30. McCusker CD, Gardiner DM. Positional Information Is Reprogrammed in Blastema
748 Cells of the Regenerating Limb of the Axolotl (Ambystoma mexicanum). Plos One.
749 2013;8(9):e77064.

750 31. Myohara M. Differential tissue development during embryogenesis and regeneration
751 in an annelid. Dev Dynam. 2004;231(2):349–58.

752 32. Schuster KJ, Smith-Bolton RK. Taranis Protects Regenerating Tissue from Fate
753 Changes Induced by the Wound Response in Drosophila. Dev Cell. 2015;34(1):119–28.

754 33. Luttrell SM, Gotting K, Ross E, Alvarado AS, Swalla BJ. Head regeneration in
755 hemichordates is not a strict recapitulation of development. Dev Dynam.
756 2016;245(12):1159–75.

757 34. Vizcaya-Molina E, Klein CC, Serras F, Mishra RK, Guigó R, Corominas M. Damage-
758 responsive elements in Drosophila regeneration. Genome Res. 2018;28(12):1852–66.

759 35. Sun G, Irvine KD. Chapter Four Control of Growth During Regeneration. Curr Top
760 Dev Biol. 2014;108:95–120.

761 36. Hariharan IK, Serras F. Imaginal disc regeneration takes flight. Curr Opin Cell Biol.
762 2017;48:10–6.

763 37. Sonoda J, Wharton RP. Drosophila Brain Tumor is a translational repressor. Gene
764 Dev. 2001;15(6):762–73.

765 38. Loedige I, Stotz M, Qamar S, Kramer K, Hennig J, Schubert T, et al. The NHL
766 domain of BRAT is an RNA-binding domain that directly contacts the hunchback mRNA
767 for regulation. Gene Dev. 2014;28(7):749–64.

768 39. Loedige I, Jakob L, Treiber T, Ray D, Stotz M, Treiber N, et al. The Crystal Structure
769 of the NHL Domain in Complex with RNA Reveals the Molecular Basis of Drosophila
770 Brain-Tumor-Mediated Gene Regulation. Cell Reports. 2015;13(6):1206–20.

771 40. Arama E, Dickman D, Kimchie Z, Shearn A, Lev Z. Mutations in the β-propeller
772 domain of the Drosophila brain tumor (brat) protein induce neoplasm in the larval brain.
773 Oncogene. 2000;19(33):1203706.

774 41. Harris RE, Pargett M, Sutcliffe C, Umulis D, Ashe HL. Brat Promotes Stem Cell
775 Differentiation via Control of a Bistable Switch that Restricts BMP Signaling. Dev Cell.
776 2011;20(1):72–83.

777 42. Betschinger J, Mechtler K, Knoblich JA. Asymmetric Segregation of the Tumor
778 Suppressor Brat Regulates Self-Renewal in Drosophila Neural Stem Cells. Cell.
779 2006;124(6):1241–53.

780 43. Lee CY, Wilkinson BD, Siegrist SE, Wharton RP, Doe CQ. Brat Is a Miranda Cargo
781 Protein that Promotes Neuronal Differentiation and Inhibits Neuroblast Self-Renewal.
782 Dev Cell. 2006;10(4):441–9.

783 44. Chen G, Kong J, Tucker-Burden C, Anand M, Rong Y, Rahman F, et al. Human Brat
784 Ortholog TRIM3 Is a Tumor Suppressor That Regulates Asymmetric Cell Division in
785 Glioblastoma. Cancer Res. 2014;74(16):4536–48.

786 45. Schwamborn JC, Berezikov E, Knoblich JA. The TRIM-NHL Protein TRIM32
787 Activates MicroRNAs and Prevents Self-Renewal in Mouse Neural Progenitors. Cell.
788 2009;136(5):913–25.

789 46. Kudryashova E, Kramerova I, Spencer MJ. Satellite cell senescence underlies
790 myopathy in a mouse model of limb-girdle muscular dystrophy 2H. J Clin Invest.
791 2012;122(5):1764–76.

792 47. Nicklas S, Otto A, Wu X, Miller P, Stelzer S, Wen Y, et al. TRIM32 Regulates
793 Skeletal Muscle Stem Cell Differentiation and Is Necessary for Normal Adult Muscle
794 Regeneration. Plos One. 2012;7(1):e30445.

795 48. Vonesch SC, Lamparter D, Mackay TFC, Bergmann S, Hafen E. Genome-Wide
796 Analysis Reveals Novel Regulators of Growth in Drosophila melanogaster. Plos Genet.
797 2016;12(1):e1005616.

798 49. Skinner A, Khan SJ, Smith-Bolton RK. Trithorax regulates systemic signaling during
799 Drosophila imaginal disc regeneration. Development. 2015;142(20):3500–11.

800 50. Khan SJ, Abidi SNF, Skinner A, Tian Y, Smith-Bolton RK. The Drosophila Duox
801 maturation factor is a key component of a positive feedback loop that sustains
802 regeneration signaling. Plos Genet. 2017;13(7):e1006937.

803 51. Brock AR, Seto M, Smith-Bolton RK. Cap-n-Collar Promotes Tissue Regeneration
804 by Regulating ROS and JNK Signaling in the Drosophila melanogaster Wing Imaginal
805 Disc. Genetics. 2017;206(3):1505–20.

806 52. Luschnig S, Moussian B, Krauss J, Desjeux I, Perkovic J, Nüsslein-Volhard C. An
807 F1 Genetic Screen for Maternal-Effect Mutations Affecting Embryonic Pattern Formation
808 in Drosophila melanogaster. Genetics. 2004;167(1):325–42.

809 53. Wright TRF, Beermann W, Marsh JL, Bishop CP, Steward R, Black BC, et al. The
810 genetics of dopa decarboxylase in Drosophila melanogaster. Chromosoma.
811 1981;83(1):45–58.

812 54. Ferreira A, Boulan L, Perez L, Milán M. Mei-P26 Mediates Tissue-Specific
813 Responses to the Brat Tumor Suppressor and the dMyc Proto-Oncogene in Drosophila.
814 Genetics. 2014;198(1):249–58.

815 55. Halme A, Cheng M, Hariharan IK. Retinoids Regulate a Developmental Checkpoint
816 for Tissue Regeneration in Drosophila. Curr Biol. 2010;20(5):458–63.

817 56. Colombani J, Andersen DS, Léopold P. Secreted Peptide Dilp8 Coordinates
818 *Drosophila* Tissue Growth with Developmental Timing. Science. 2012;336(6081):582–5.

819 57. Garelli A, Gontijo AM, Miguela V, Caparros E, Dominguez M. Imaginal Discs
820 Secrete Insulin-Like Peptide 8 to Mediate Plasticity of Growth and Maturation. Science.
821 2012;336(6081):579–82.

822 58. Abbott LC, Karpen GH, Schubiger G. Compartmental restrictions and blastema
823 formation during pattern regulation in Drosophila imaginal leg discs. Dev Biol.
824 1981;87(1):64–75.

825 59. Ng M, Diaz-Benjumea FJ, Cohen SM. Nubbin encodes a POU-domain protein
826 required for proximal-distal patterning in the Drosophila wing. Dev Camb Engl.
827 1995;121(2):589–99.

828 60. Komori H, Xiao Q, McCartney BM, Lee CY. Brain tumor specifies intermediate
829 progenitor cell identity by attenuating β-catenin/Armadillo activity. Development.
830 2014;141(1):51–62.

831 61. Couso J, Bate M, Martinez-Arias A. A wingless-dependent polar coordinate system
832 in Drosophila imaginal discs. Science. 1993;259(5094):484–9.

833 62. Wu DC, Johnston LA. Control of Wing Size and Proportions by Drosophila Myc.
834 Genetics. 2010;184(1):199–211.

835 63. Diaz-Benjumea FJ, Cohen SM. Interaction between dorsal and ventral cells in the
836 imaginal disc directs wing development in Drosophila. Cell. 1993;75(4):741–52.

837 64. Micchelli CA, Rulifson EJ, Blair SS. The function and regulation of cut expression on
838 the wing margin of Drosophila: Notch, Wingless and a dominant negative role for Delta
839 and Serrate. Dev Camb Engl. 1997;124(8):1485–95.

840 65. Becam I, Milán M. A permissive role of Notch in maintaining the DV affinity
841 boundary of the Drosophila wing. Dev Biol. 2008;322(1):190–8.

842 66. Saj A, Arziman Z, Stempfle D, Belle W van, Sauder U, Horn T, et al. A Combined Ex
843 Vivo and In Vivo RNAi Screen for Notch Regulators in Drosophila Reveals an Extensive
844 Notch Interaction Network. Dev Cell. 2010;18(5):862–76.

845 67. Mukherjee S, Tucker-Burden C, Zhang C, Moberg K, Read R, Hadjipanayis C, et al.
846 Drosophila Brat and Human Ortholog TRIM3 Maintain Stem Cell Equilibrium and
847 Suppress Brain Tumorigenesis by Attenuating Notch Nuclear Transport. Cancer Res.
848 2016;76(8):2443–52.

849 68. Couso JP, Bishop SA, Arias AM. The wingless signalling pathway and the
850 patterning of the wing margin in Drosophila. Dev Camb Engl. 1994;120(3):621–36.

851 69. Jack J, Dorsett D, Delotto Y, Liu S. Expression of the cut locus in the Drosophila
852 wing margin is required for cell type specification and is regulated by a distant
853 enhancer. Dev Camb Engl. 1991;113(3):735–47.

854 70. Pierce SB, Yost C, Britton JS, Loo LWM, Flynn EM, Edgar BA, et al. dMyc is
855 required for larval growth and endoreplication in Drosophila. Development.
856 2004;131(10):2317–27.

857 71. Bosch JA, Sumabat TM, Hariharan IK. Persistence of RNAi-Mediated Knockdown in
858 Drosophila Complicates Mosaic Analysis Yet Enables Highly Sensitive Lineage Tracing.
859 Genetics. 2016;203(1):109–18.

860 72. Johnston LA, Prober DA, Edgar BA, Eisenman RN, Gallant P. Drosophila myc
861 Regulates Cellular Growth during Development. Cell. 1999;98(6):779–90.

862 73. Dillard C, Narbonne-Reveau K, Foppolo S, Lanet E, Maurange C. Two distinct
863 mechanisms silence chinmo in Drosophila neuroblasts and neuroepithelial cells to limit
864 their self-renewal. Development. 2017;145(2):dev.154534.

865 74. Flaherty MS, Salis P, Evans CJ, Ekas LA, Marouf A, Zavadil J, et al. chinmo Is a
866 Functional Effector of the JAK/STAT Pathway that Regulates Eye Development, Tumor
867 Formation, and Stem Cell Self-Renewal in Drosophila. Dev Cell. 2010;18(4):556–68.

868 75. Narbonne-Reveau K, Maurange C. Developmental regulation of regenerative
869 potential in Drosophila by ecdysone through a bistable loop of ZBTB transcription
870 factors. Plos Biol. 2019;17(2):e3000149.

871 76. Kudron MM, Victorsen A, Gevirtzman L, Hillier LW, Fisher WW, Vafeados D, et al.
872 The modERN Resource: Genome-Wide Binding Profiles for Hundreds of Drosophila
873 and Caenorhabditis elegans Transcription Factors. Genetics.
874 2017;208(3):genetics.300657.2017.

875 77. Yang J, Sung E, Donlin-Asp PG, Corces VG. A subset of Drosophila Myc sites
876 remain associated with mitotic chromosomes co-localized with insulator proteins. Nat
877 Commun. 2013;4(1):1464–1464.

878 78. Sitaram P, Lu S, Harsh S, Herrera SC, Bach EA. Next-Generation Sequencing
879 Reveals Increased Anti-oxidant Response and Ecdysone Signaling in STAT
880 Supercompetitors in Drosophila. G3 Genes Genomes Genetics. 2019;9(8):2609–22.

881 79. Narbonne-Reveau K, Maurange C. Developmental regulation of regenerative
882 potential in Drosophila by ecdysone through a bistable loop of ZBTB transcription
883 factors. Plos Biol. 2019;17(2):e3000149.

884 80. Amati B, Land H. Myc—Max—Mad: a transcription factor network controlling cell
885 cycle progression, differentiation and death. Curr Opin Genet Dev. 1994;4(1):102–8.

886 81. Takahashi K, Yamanaka S. Induction of Pluripotent Stem Cells from Mouse
887 Embryonic and Adult Fibroblast Cultures by Defined Factors. Cell. 2006;126(4):663–76.

888 82. Marygold SJ, Coelho CMA, Leevers SJ. Genetic Analysis of RpL38 and RpL5, Two
889 Minute Genes Located in the Centric Heterochromatin of Chromosome 2 of Drosophila
890 melanogaster. Genetics. 2005;169(2):683–95.

891 83. Tian Y, Smith-Bolton RK. Regulation of growth and cell fate during tissue
892 regeneration by the two SWI/SNF chromatin-remodeling complexes of Drosophila.
893 Genetics. 2020;217(1):iyaa028.

894 84. Hayashi R, Goto Y, Ikeda R, Yokoyama KK, Yoshida K. CDCA4 Is an E2F
895 Transcription Factor Family-induced Nuclear Factor That Regulates E2F-dependent
896 Transcriptional Activation and Cell Proliferation. J Biol Chem. 2006;281(47):35633–48.

897 85. Hsu SI, Yang CM, Sim KG, Hentschel DM, O'Leary E, Bonventre JV. TRIP-Br: a
898 novel family of PHD zinc finger- and bromodomain-interacting proteins that regulate the
899 transcriptional activity of E2F-1/DP-1. Embo J. 2001;20(9):2273–85.

900 86. Watanabe-Fukunaga R, Iida S, Shimizu Y, Nagata S, Fukunaga R. SEI family of
901 nuclear factors regulates p53-dependent transcriptional activation. Genes Cells.
902 2005;10(8):851–60.

903 87. Calgaro S, Boube M, Cribbs DL, Bourbon HM. The Drosophila gene taranis
904 encodes a novel trithorax group member potentially linked to the cell cycle regulatory
905 apparatus. Genetics. 2002;160(2):547–60.

906 88. Laver JD, Li X, Ray D, Cook KB, Hahn NA, Nabeel-Shah S, et al. Brain tumor is a
907 sequence-specific RNA-binding protein that directs maternal mRNA clearance during
908 the Drosophila maternal-to-zygotic transition. Genome Biol. 2015;16(1):94.

909 89. Komori H, Golden KL, Kobayashi T, Kageyama R, Lee CY. Multilayered gene
910 control drives timely exit from the stem cell state in uncommitted progenitors during
911 Drosophila asymmetric neural stem cell division. Gene Dev. 2018;32(23–24):1550–61.

912 90. Hazelrigg T, Levis R, Rubin GM. Transformation of white locus DNA in Drosophila:
913 Dosage compensation, zeste interaction, and position effects. Cell. 1984;36(2):469–81.

914 91. Wright TR, Bewley GC, Sherald AF. The genetics of dopa decarboxylase in
915 Drosophila melanogaster. II. Isolation and characterization of dopa-decarboxylase-
916 deficient mutants and their relationship to the alpha-methyl-dopa-hypersensitive
917 mutants. Genetics. 1976;84(2):287–310.

918 92. Parks AL, Cook KR, Belvin M, Dompe NA, Fawcett R, Huppert K, et al. Systematic
919 generation of high-resolution deletion coverage of the Drosophila melanogaster
920 genome. Nat Genet. 2004;36(3):ng1312.

921 93. Stathakis DG, Pentz ES, Freeman ME, Kullman J, Hankins GR, Pearlson NJ, et al.
922 The genetic and molecular organization of the Dopa decarboxylase gene cluster of
923 Drosophila melanogaster. Genetics. 1995;141(2):629–55.

924 94. Cohen B, McGuffin ME, Pfeifle C, Segal D, Cohen SM. apterous, a gene required
925 for imaginal disc development in Drosophila encodes a member of the LIM family of
926 developmental regulatory proteins. Gene Dev. 1992;6(5):715–29.

927 95. Littleton JT, Bellen HJ. Genetic and phenotypic analysis of thirteen essential genes
928 in cytological interval 22F1-2; 23B1-2 reveals novel genes required for neural
929 development in Drosophila. Genetics. 1994;138(1):111–23.

930 96. Averof M, Cohen SM. Evolutionary origin of insect wings from ancestral gills.
931 Nature. 1997;385(6617):385627a0.

932 97. Classen AK, Bunker BD, Harvey KF, Vaccari T, Bilder D. A tumor suppressor
933 activity of Drosophila Polycomb genes mediated by JAK-STAT signaling. Nat Genet.
934 2009;41(10):1150–5.

98. Mitchell NC, Johanson TM, Cranna NJ, Er ALJ, Richardson HE, Hannan RD, et al. Hfp inhibits Drosophila myc transcription and cell growth in a TFIIH/Hay-dependent manner. Development. 2010;137(17):2875–84.

Figure 1

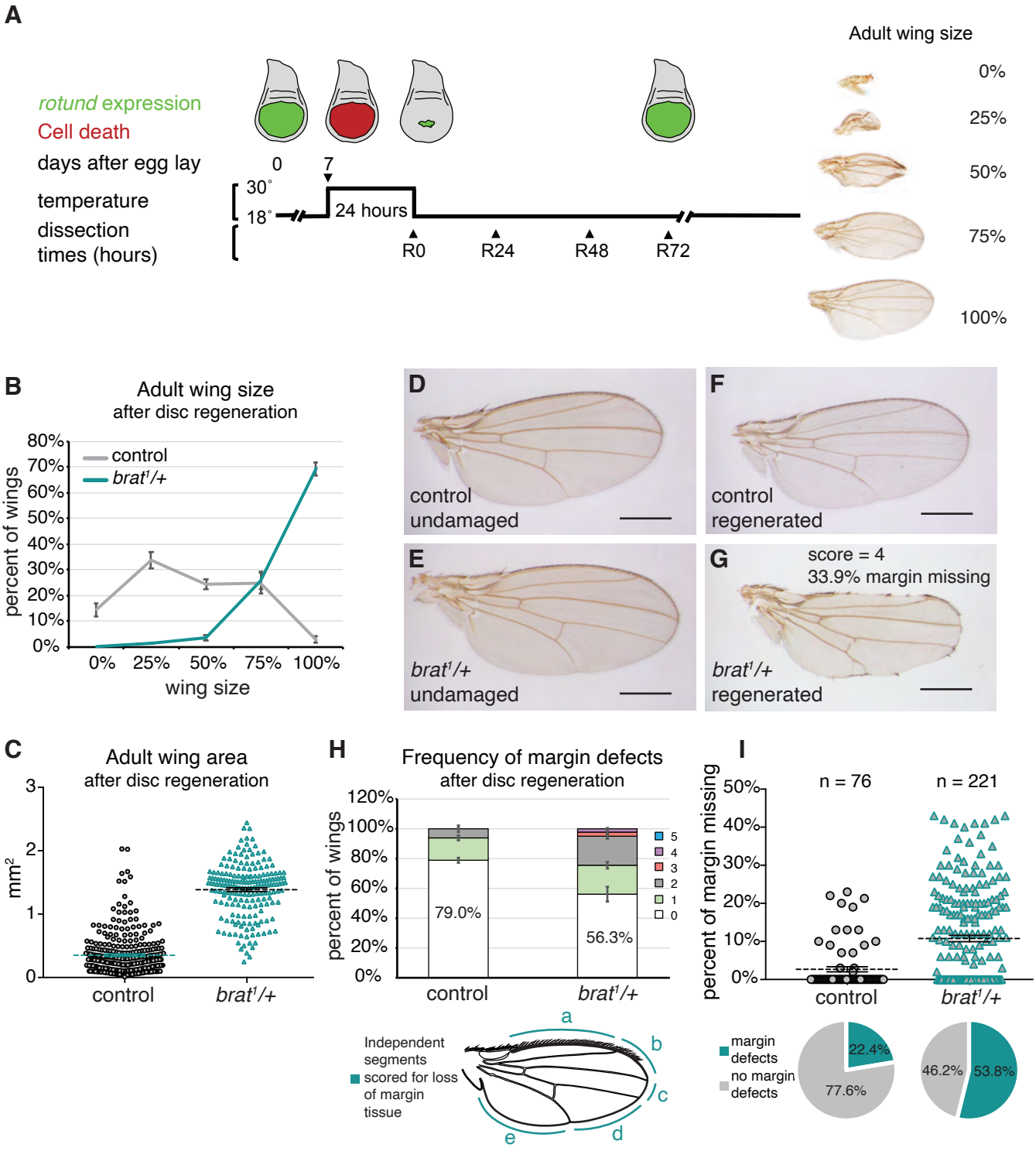
A
rotund expression
Cell death
days after egg lay
0
7
temperature
30˚
18˚
24 hours
dissection times (hours)
R0
R24
R48
R72
Adult wing size
0%
25%
50%
75%
100%
B
Adult wing size
after disc regeneration
control
brat1/+
percent of wings
80%
70%
60%
50%
40%
30%
20%
10%
0%
0%
25%
50%
75%
100%
wing size
D
control
undamaged
F
control
regenerated
E
brat1/+
undamaged
G
score = 4
33.9% margin missing
brat1/+
regenerated
C
Adult wing area
after disc regeneration
mm2
3
2
1
0
control
brat1/+
H
Frequency of margin defects
after disc regeneration
percent of wings
120%
100%
80%
60%
40%
20%
0%
79.0%
56.3%
5
4
3
2
1
0
control
brat1/+
Independent segments scored for loss of margin tissue
a
b
c
d
e
I
n = 76
n = 221
percent of margin missing
50%
40%
30%
20%
10%
0%
control
brat1/+
margin defects
no margin defects
22.4%
77.6%
46.2%
53.8%

940 **Figure 1. Enhanced regenerative growth and wing margin cell-fate specification**
941 **defects in *brat*^{1}/+ during regeneration.**

942 (A) The protocol used to study regeneration. Animals were raised at 18°C and shifted to
943 30°C for 24 hours during early third-instar larval development on day 7 after egg lay
944 (AEL). Larvae were returned to 18°C and were dissected at the time points noted during
945 recovery (R) or allowed to pupariate and eclose. Representative wings depicting the
946 range of adult wing sizes observed after regeneration compared to the size of a normal
947 wing are shown. (B) Adult wing sizes observed after disc regeneration for control (w^{1118})
948 (n = 317) and *brat*^{1}/+ (n = 208) wings, from three independent experiments. (C) Adult
949 wing area after disc regeneration, measured using ImageJ after mounting and imaging
950 wings, for control (w^{1118}) (n = 309) and *brat*^{1}/+ (n = 195) wings. p = 2.5158E-119. Wings
951 in (C) are from the same experiments as (B). Note that number of wings in (C) is less for
952 both control and *brat*^{1}/+ due to some wings being damaged during the mounting
953 process. (D) Undamaged control (w^{1118}) wing. (E) Undamaged *brat*^{1}/+ wing. (F) Adult
954 control (w^{1118}) wing after disc regeneration. (G) Adult *brat*^{1}/+ wing after disc
955 regeneration. (H) Frequency of margin defects seen in adult wings after disc
956 regeneration for control (w^{1118}) (n = 93) and *brat*^{1}/+ (n = 218) wings, from three
957 independent experiments. The wing margin was divided into five segments based on
958 where the veins intersect the margin as shown in the diagram. Each wing was scored
959 for the number of segments that had some margin tissue missing, with wings with a
960 perfectly intact margin scoring at zero. Wing shown in (G) had tissue missing in four
961 segments. (I) Margin tissue lost as a percentage of total wing perimeter for control
962 (w^{1118}) (n = 76) and *brat*^{1}/+ (n = 221) wings. p = 9.947E-08. The margin perimeter and
963 the length of margin tissue lost were measured using ImageJ after mounting and

964 imaging wings. Wings in (I) are from the same experiments as (H). Note that number of
965 wings in the two quantifications is different because we did not quantify wings with
966 length <1.1 mm for males and <1.7 mm for females, to ensure analysis was being
967 carried out on nearly fully regenerated wings. (I). Percentage of wings with no defects
968 fell from 79.0% to 77.6% for control and from 56.3% to 53.8% for *brat*^{1}/+ wings due to
969 the increased ability to detect lost margin tissue at the higher magnification and
970 resolution achieved by imaging the wings. Wing shown in (G) had 33.9% of margin
971 tissue missing. Error bars mark standard error of the mean (SEM). Student's T-test
972 used for statistical analyses. Scale bars are 0.5 mm.

Figure 2

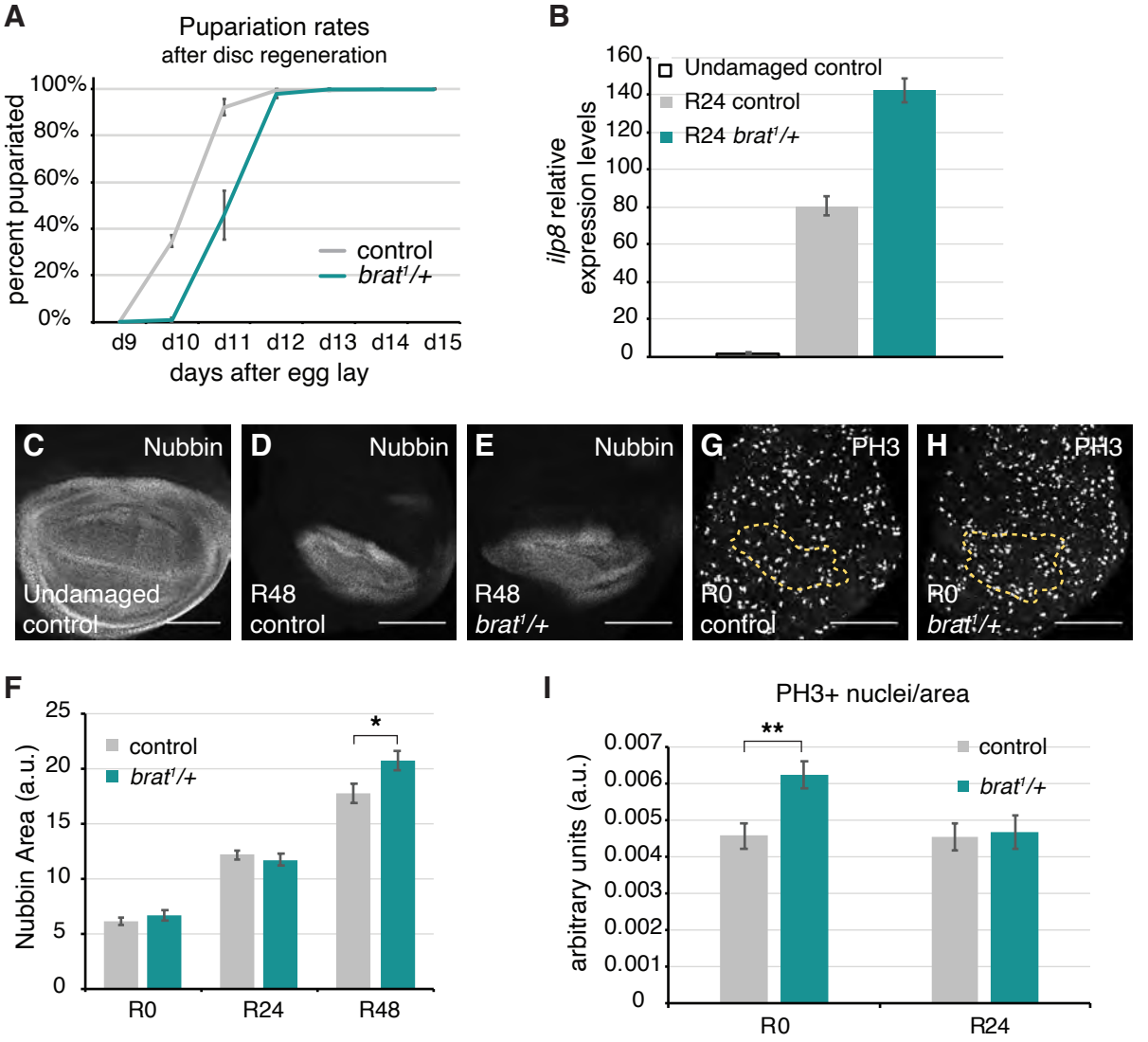
A
Pupariation rates
after disc regeneration
percent pupariated
100%
80%
60%
40%
20%
0%
d9
d10
d11
d12
d13
d14
d15
days after egg lay
control
brat1/+
B
ilp8 relative expression levels
160
140
120
100
80
60
40
20
0
Undamaged control
R24 control
R24 brat1/+
C
Nubbin
Undamaged control
D
Nubbin
R48 control
E
Nubbin
R48 brat1/+
G
PH3
R0 control
H
PH3
R0 brat1/+
F
Nubbin Area (a.u.)
25
20
15
10
5
0
control
brat1/+
*
R0
R24
R48
I
PH3+ nuclei/area
arbitrary units (a.u.)
0.007
0.006
0.005
0.004
0.003
0.002
0.001
0
**
control
brat1/+
R0
R24

973 **Figure 2. *brat^{1}*/+ animals have a regenerative growth advantage.**

974 (A) Pupariation rates after disc regeneration for control (*w^{1118}*) (n = 384) and *brat^{1}*/+ (n =
975 107) animals, from three independent experiments. (B) Relative expression levels of
976 *ilp8* for undamaged control, R24 control (*w^{1118}*) and R24 *brat^{1}*/+ discs. (C) Anti-Nubbin
977 immunostaining in an undamaged control disc. (D-E) Anti-Nubbin immunostaining in an
978 R48 control (*w^{1118}*) disc (D), and an R48 *brat^{1}*/+ disc (E). (F) Quantification of area of
979 Nubbin-expressing cells for control (*w^{1118}*) and *brat^{1}*/+ discs at R0 (n = 10 and 10), R24
980 (n = 12 and 12) and R48 (n = 10 and 10). * $p < 0.03$. (G-H) Anti-PH3 immunostaining in
981 an R0 control (*w^{1118}*) disc (G), and an R0 *brat^{1}*/+ disc (H). The yellow dashed lines
982 outline the Nubbin-expressing wing pouch. (I) PH3-positive nuclei were counted within
983 the regenerating tissue as marked by Anti-Nubbin co-immunostaining. Quantification of
984 PH3-positive nuclei in Nubbin area for control (*w^{1118}*) and *brat^{1}*/+ discs at R0 (n = 16 and
985 18) and R24 (n = 15 and 16). ** $p < 0.002$. Error bars represent SEM. Student's T-test
986 used for statistical analyses. Scale bars are 100 μm.

Figure 3

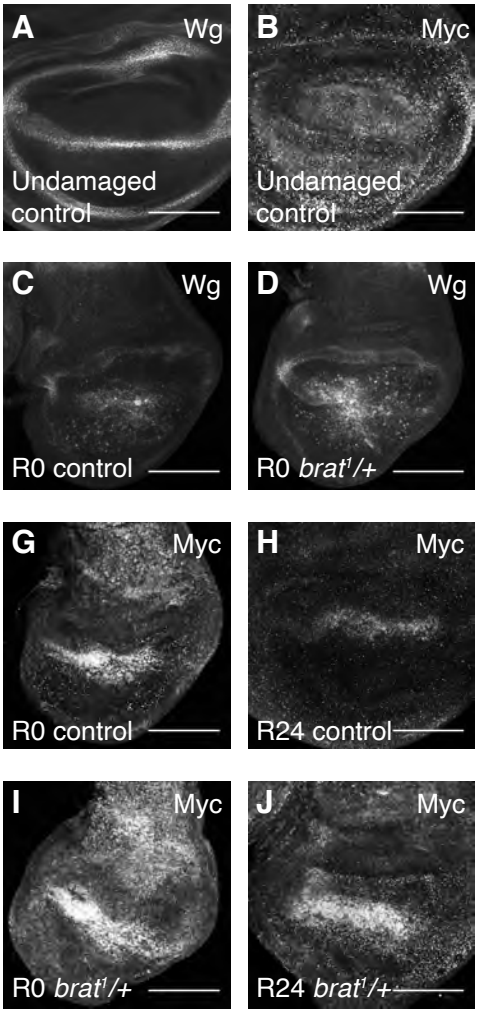
A
Wg
Undamaged control
B
Myc
Undamaged control
C
Wg
R0 control
D
Wg
R0 brat¹/+
G
Myc
R0 control
H
Myc
R24 control
I
Myc
R0 brat¹/+
J
Myc
R24 brat¹/+

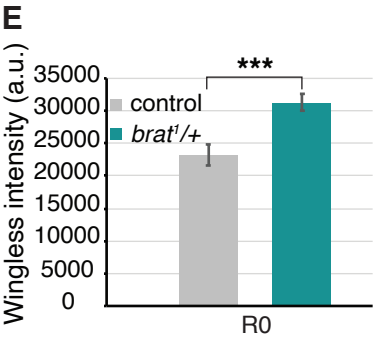
E
Wingless intensity (a.u.)
35000
30000
25000
20000
15000
10000
5000
0
control
brat¹/+
***
R0

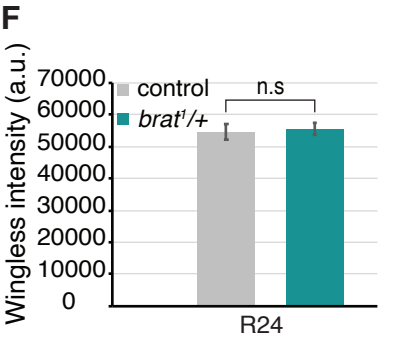
F
Wingless intensity (a.u.)
70000
60000
50000
40000
30000
20000
10000
0
control
brat¹/+
n.s
R24

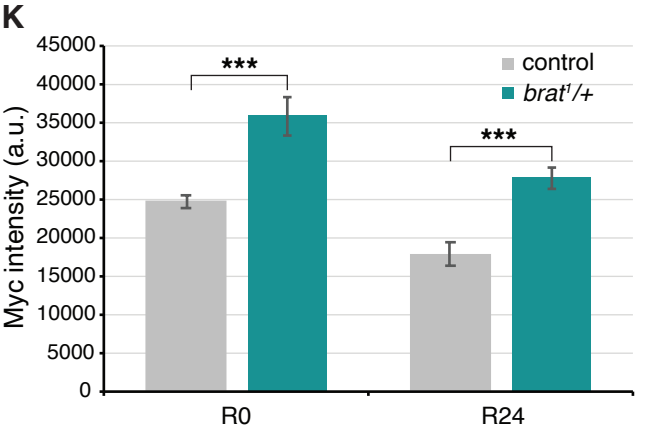
K
Myc intensity (a.u.)
45000
40000
35000
30000
25000
20000
15000
10000
5000
0
control
brat¹/+
***
***
R0
R24

987 **Figure 3. *brat^{1}*/+ animals experience elevated regeneration signaling.**

988 (A) Anti-Wg immunostaining in an undamaged control (*w^{1118}*) disc. (B) Anti-Myc
989 immunostaining in an undamaged control (*w^{1118}*) disc. (C-D) Anti-Wg immunostaining in
990 an R0 control (*w^{1118}*) disc (C) and an R0 *brat^{1}*/+ disc (D). (E) Quantification of Wg
991 fluorescence intensity in R0 control (*w^{1118}*) (n = 13) and R0 *brat^{1}*/+ (n = 17) discs. *** $p <$
992 0.0006. (F) Quantification of Wg fluorescence intensity in R24 control (*w^{1118}*) (n = 12)
993 and R24 *brat^{1}*/+ (n = 11) discs. Area for fluorescence intensity measurement was
994 defined by the Wg expression domain in the wing pouch. (G-J) Anti-Myc
995 immunostaining in an R0 control (*w^{1118}*) disc (G), an R24 control (*w^{1118}*) disc (H), an R0
996 *brat^{1}*/+ disc (I) and an R24 *brat^{1}*/+ disc (J). (K) Quantification of Myc fluorescence
997 intensity in R0 control (*w^{1118}*) (n = 13), R0 *brat^{1}*/+ (n = 12), R24 control (*w^{1118}*) (n = 13),
998 and R24 *brat^{1}*/+ (n = 12) discs. Area for fluorescence intensity measurement was
999 defined by the elevated Myc expression domain in the wing pouch. R0 *** $p < 0.0003$,
1000 R24 *** $p < 0.0001$. Error bars represent SEM. Student's T-test used for statistical
1001 analyses. Scale bars are 100 μm.

Figure 4

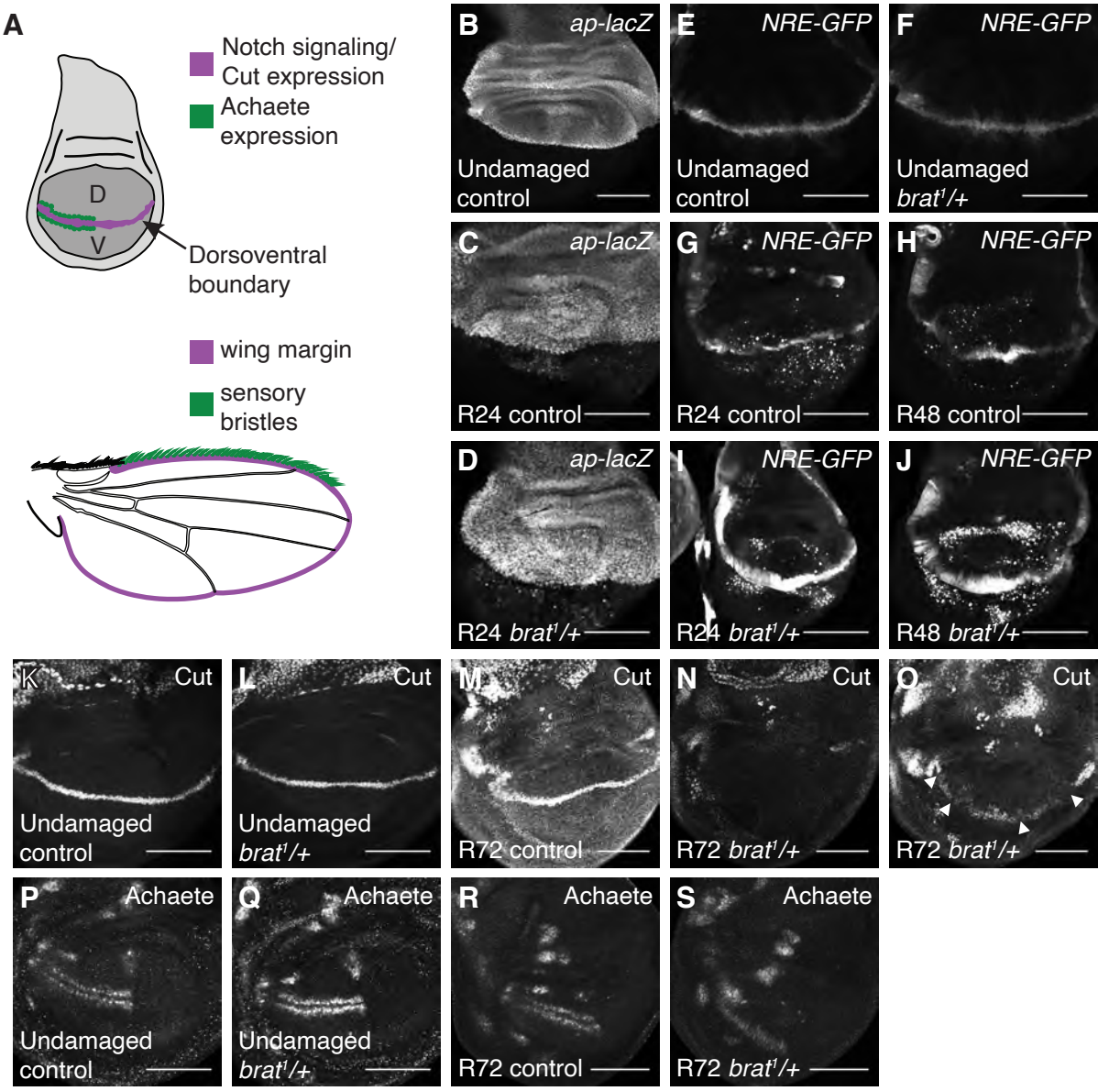
A
Notch signaling/ Cut expression
Achaete expression
D
V
Dorsoventral boundary
wing margin
sensory bristles
B ap-lacZ
Undamaged control
E NRE-GFP
Undamaged control
F NRE-GFP
Undamaged brat1/+
C ap-lacZ
R24 control
G NRE-GFP
R24 control
H NRE-GFP
R48 control
D ap-lacZ
R24 brat1/+
I NRE-GFP
R24 brat1/+
J NRE-GFP
R48 brat1/+
K Cut
Undamaged control
L Cut
Undamaged brat1/+
M Cut
R72 control
N Cut
R72 brat1/+
O Cut
R72 brat1/+
P Achaete
Undamaged control
Q Achaete
Undamaged brat1/+
R Achaete
R72 control
S Achaete
R72 brat1/+

1002 **Figure 4. *Brat* regulates margin cell-fate specification.**

1003 (A) Drawings of a wing imaginal disc and an adult wing. D = dorsal and V = ventral
1004 compartments of the wing disc, with the dorsoventral boundary marked in purple. Notch
1005 signaling and Cut expression are present at the dorsoventral boundary, which forms the
1006 adult wing margin, also marked in purple. Achaete-expressing cells, marked in green,
1007 give rise to the sensory bristles at the anterior half of the margin in the adult wing, also
1008 marked in green. (B) *ap-lacZ* expression in an undamaged control disc from a third-
1009 instar *ap-lacZ/CyO* animal. (C-D) *ap-lacZ* expression in an R24 control (w^{1118}) disc (C)
1010 and an R24 $brat^{1}$/+ disc (D). (E-F) *NRE-GFP* expression in an undamaged control
1011 (w^{1118}) disc (E) and an undamaged $brat^{1}$/+ disc (F). (G-J) *NRE-GFP* expression in an
1012 R0 control (w^{1118}) disc (G), an R24 control (w^{1118}) disc (H), an R0 $brat^{1}$/+ disc (I) and an
1013 R24 $brat^{1}$/+ disc (J). (K-L) Anti-Ct immunostaining in an undamaged control (w^{1118}) disc
1014 (K) and an undamaged $brat^{1}$/+ disc (L). (M-O) Anti-Ct immunostaining in an R72 control
1015 (w^{1118}) disc (M) and an R72 $brat^{1}$/+ discs (N-O). Arrowheads point to loss of Ct
1016 expression in (O). (P-Q) Anti-Ac immunostaining in an undamaged control (w^{1118}) disc
1017 (P) and an undamaged $brat^{1}$/+ disc (Q). (R-S) Anti-Ac immunostaining in an R72 control
1018 (w^{1118}) disc (R) and an R72 $brat^{1}$/+ disc (S). Scale bars are 100 μm.

Figure 5

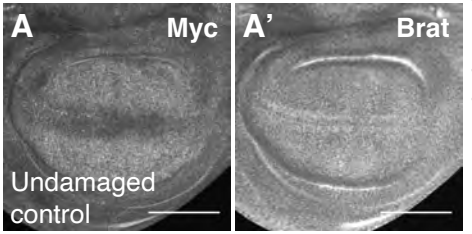
A
Myc
Undamaged control
A'
Brat

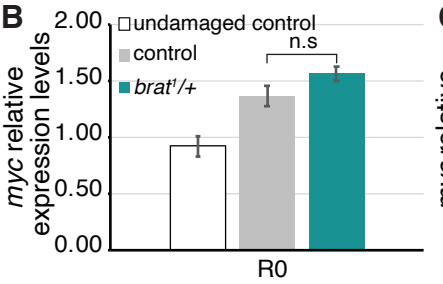
B
undamaged control
control
brat¹/+
n.s
myc relative expression levels
2.00
1.50
1.00
0.50
0.00
R0

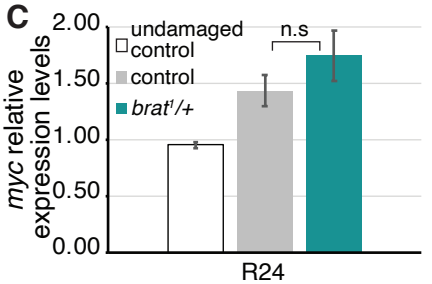
C
undamaged control
control
brat¹/+
n.s
myc relative expression levels
2.00
1.50
1.00
0.50
0.00
R24

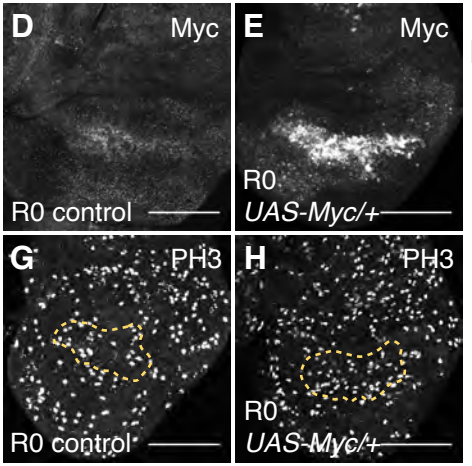
D
Myc
R0 control
E
Myc
R0
UAS-Myc/+
G
PH3
R0 control
H
PH3
R0
UAS-Myc/+

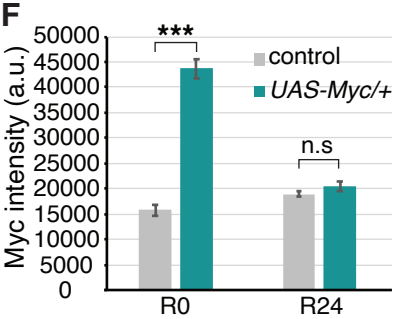
F
***
control
UAS-Myc/+
n.s
Myc intensity (a.u.)
50000
45000
40000
35000
30000
25000
20000
15000
10000
5000
0
R0
R24

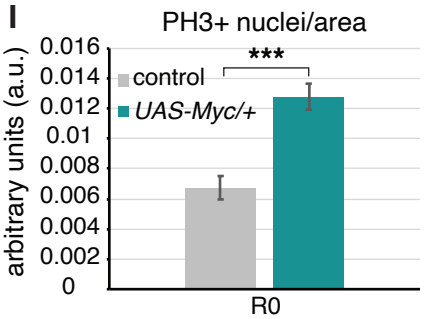
I
PH3+ nuclei/area
***
control
UAS-Myc/+
arbitrary units (a.u.)
0.016
0.014
0.012
0.01
0.008
0.006
0.004
0.002
0
R0

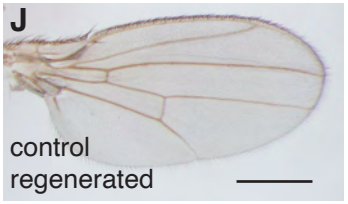
J
control
regenerated

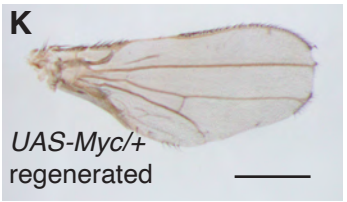
K
UAS-Myc/+
regenerated

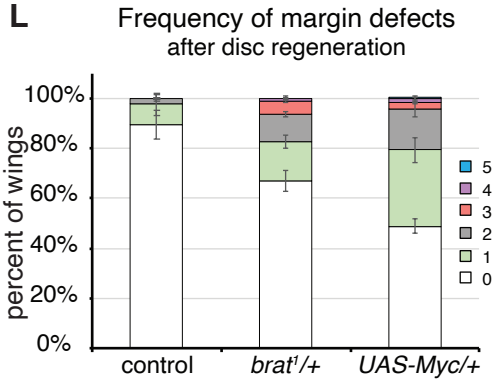
L
Frequency of margin defects
after disc regeneration
percent of wings
100%
80%
60%
40%
20%
0%
control
brat¹/+
UAS-Myc/+
5
4
3
2
1
0

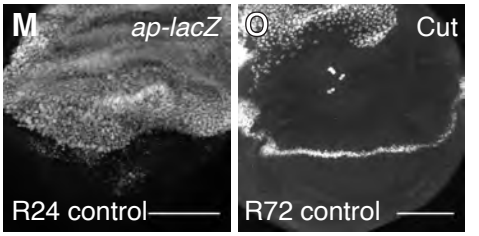
M
ap-lacZ
R24 control
O
Cut
R72 control

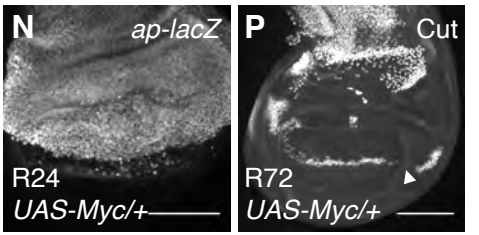
N
ap-lacZ
R24
UAS-Myc/+
P
Cut
R72
UAS-Myc/+

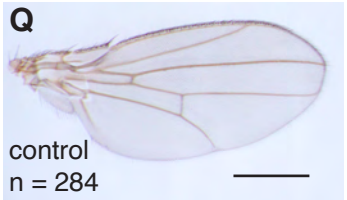
Q
control
n = 284

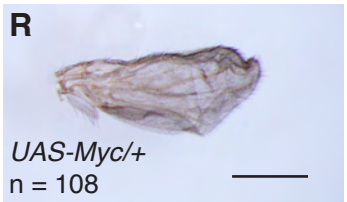
R
UAS-Myc/+
n = 108

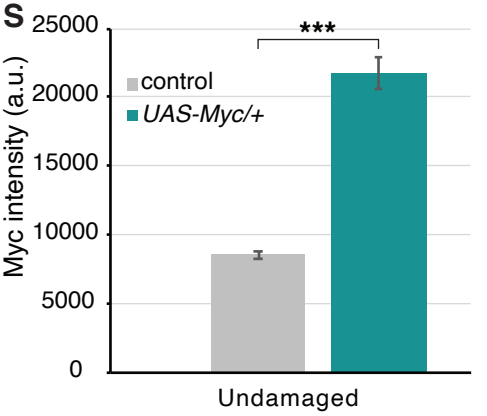
S
***
control
UAS-Myc/+
Myc intensity (a.u.)
25000
20000
15000
10000
5000
0
Undamaged

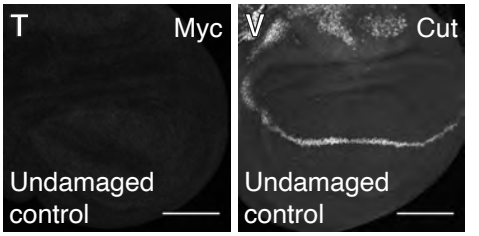
T
Myc
Undamaged control
V
Cut
Undamaged control

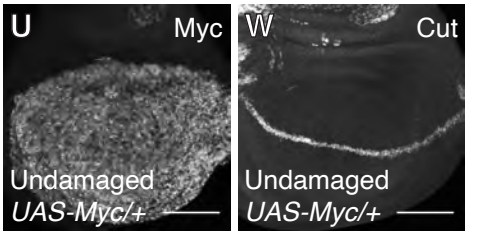
U
Myc
Undamaged
UAS-Myc/+
W
Cut
Undamaged
UAS-Myc/+

1019 **Figure 5. High Myc expression causes margin defects.**

1020 (A-A') Anti-Myc and Anti-Brat co-immunostaining in an undamaged control disc.
1021 *rnGAL4, GAL80^{ts}/attP2* animals were shifted to 30°C on day 7 AEL and dissected 24
1022 hours later. (B-C) Relative expression levels of *myc* for undamaged control,
1023 regenerating control (*w^{1118}*), and regenerating *brat^{1}*/+ discs at R0 (B) and R24 (C). P
1024 values for comparison between regenerating control and *brat^{1}*/+ discs: $p > 0.1$ at R0,
1025 and $p > 0.3$ at R24. (D-E) Anti-Myc immunostaining in an R0 control (*w^{1118}*) disc (D) and
1026 an R0 *UAS-Myc/*+ disc (E). (F) Quantification of Myc fluorescence intensity in R0 control
1027 (*w^{1118}*) (n = 13), R0 *UAS-Myc/*+ (n = 12), R24 control (*w^{1118}*) (n = 13), and R24 *UAS-*
1028 *Myc/*+ (n = 12) discs. Area for fluorescence intensity measurement was defined by the
1029 elevated Myc expression domain in the wing pouch. *** p = 1.2E-11. (G-H) Anti-PH3
1030 immunostaining in an R0 control (*w^{1118}*) disc (G), and an R0 *UAS-Myc/*+ disc (H). The
1031 yellow dashed lines outline the Nubbin-expressing wing pouch. (I) PH3-positive nuclei
1032 were counted within the regenerating wing pouch as marked by Anti-Nubbin co-
1033 immunostaining. Quantification of PH3-positive nuclei in the Nubbin area for R0 control
1034 (*w^{1118}*) (n = 15) and *UAS-Myc/*+ (n = 15) discs. *** $p < 0.00002$. (J) Adult control (*w^{1118}*)
1035 wing after disc regeneration. (K) Adult *UAS-Myc/*+ wing after disc regeneration. (L)
1036 Frequency of margin defects, as quantified in Figure 1H, seen in adult wings after disc
1037 regeneration for control (*w^{1118}*) (n = 134), *brat^{1}*/+ (n = 193) and *UAS-Myc/*+ (n = 200)
1038 wings, from three independent experiments. (M-N) *ap-lacZ* expression in an R24 control
1039 (*w^{1118}*) disc (M) and an R24 *UAS-Myc/*+ disc (N). (O-P) Anti-Ct immunostaining in an
1040 R72 control (*w^{1118}*) disc (O) and an R72 *UAS-Myc/*+ disc (P). (Q) Adult undamaged
1041 control (+*; rnGAL4,GAL80ts/*+) wing from animals shifted to 30°C on day 7 AEL and

1042 maintained at 30°C until eclosion. (R) Adult wing from discs continuously
1043 overexpressing Myc from day 7 AEL onwards (*UAS-Myc/+; rnGAL4, GAL80ts/+)*. (S)
1044 Quantification of Myc fluorescence intensity in undamaged discs dissected 31 hours
1045 after animals were shifted to 30°C on day 7 AEL. Control (+*; rnGAL4,GAL80ts/*+) (n =
1046 14) and *UAS-Myc (UAS-Myc/+; rnGAL4, GAL80ts/+)* (n = 14). Area for fluorescence
1047 intensity measurement was defined by the Myc expression domain in the wing pouch.
1048 *** p = 1.2E-11. (T-U) Anti-Myc immunostaining in an undamaged control disc (T) and
1049 an undamaged *UAS-Myc/*+ disc (U). (V-W) Anti-Ct immunostaining in an undamaged
1050 control disc (V) and an undamaged *UAS-Myc/*+ disc (W). Error bars represent SEM.
1051 Student's T-test used for statistical analyses. Scale bars are 100 μm. Scale bars for
1052 adult wings are 0.5 mm.

Figure 6

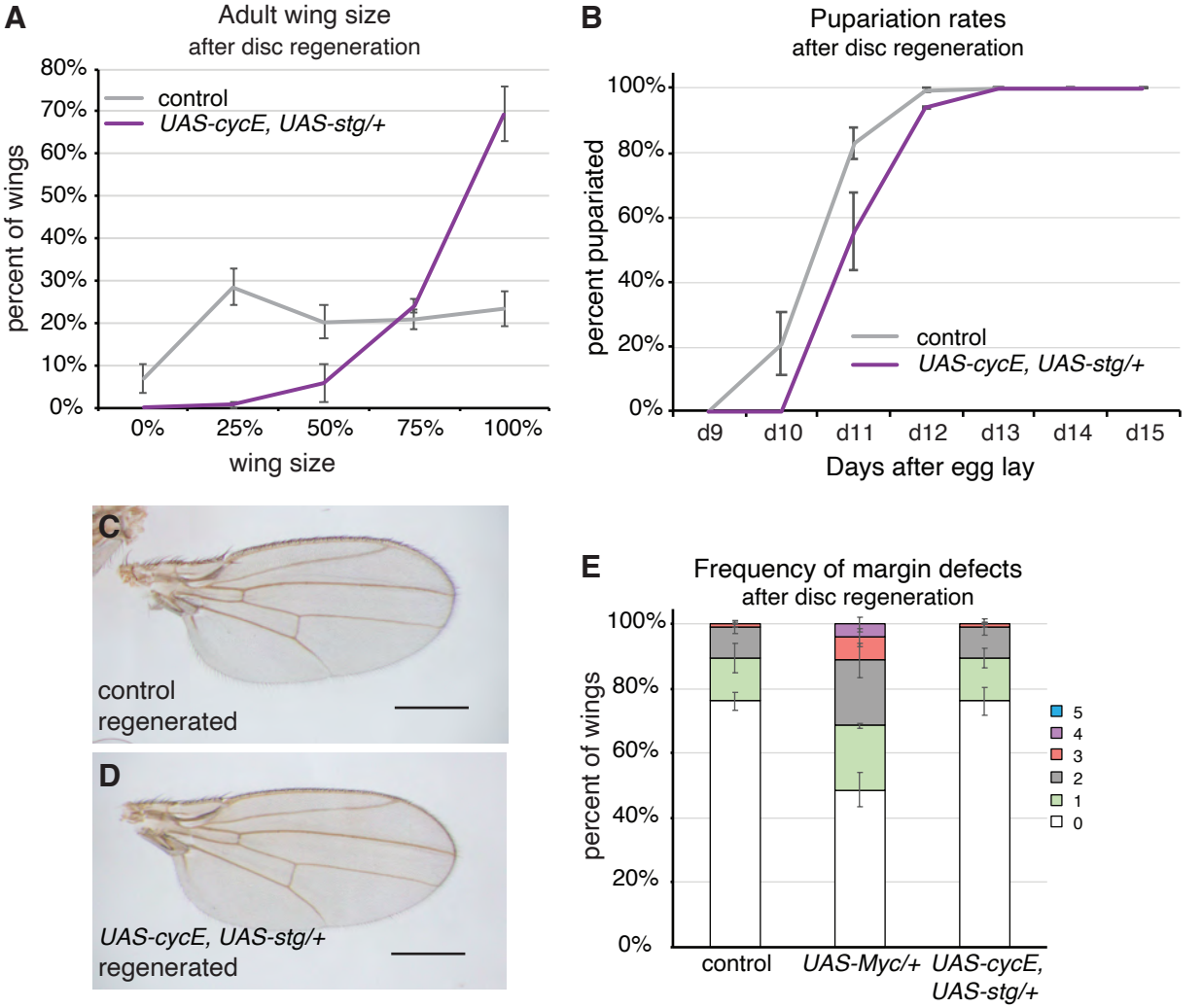
A
Adult wing size
after disc regeneration
80%
70%
60%
50%
40%
30%
20%
10%
0%
percent of wings
control
UAS-cycE, UAS-stg/+
0%
25%
50%
75%
100%
wing size
B
Pupariation rates
after disc regeneration
100%
80%
60%
40%
20%
0%
percent pupariated
control
UAS-cycE, UAS-stg/+
d9
d10
d11
d12
d13
d14
d15
Days after egg lay
C
control
regenerated
D
UAS-cycE, UAS-stg/+
regenerated
E
Frequency of margin defects
after disc regeneration
100%
80%
60%
40%
20%
0%
percent of wings
5
4
3
2
1
0
control
UAS-Myc/+
UAS-cycE,
UAS-stg/+

1053 **Figure 6. Overexpression of cell cycle genes does not cause patterning defects.**

1054 (A) Adult wing sizes observed after disc regeneration for control (w^{1118}) (n = 280) and
1055 *UAS-cycE, UAS-stg/+* (n = 194) wings, from three independent experiments. (B)
1056 Pupariation rates after disc regeneration for control (w^{1118}) (n = 174) and *UAS-cycE,*
1057 *UAS-stg/+* (n = 115) wings, from three independent experiments. (C) Adult control
1058 (w^{1118}) wing after disc regeneration. (D) Adult *UAS-cycE, UAS-stg/+* wing after disc
1059 regeneration. (E) Frequency of margin defects seen in adult wings after disc
1060 regeneration for control (w^{1118}) (n = 118), *UAS-Myc/+* (n = 146), and *UAS-cycE, UAS-*
1061 *stg/+* (n = 188) wings, from three independent experiments. Error bars represent SEM.
1062 Scale bars for adult wings are 0.5 mm.

Figure 7

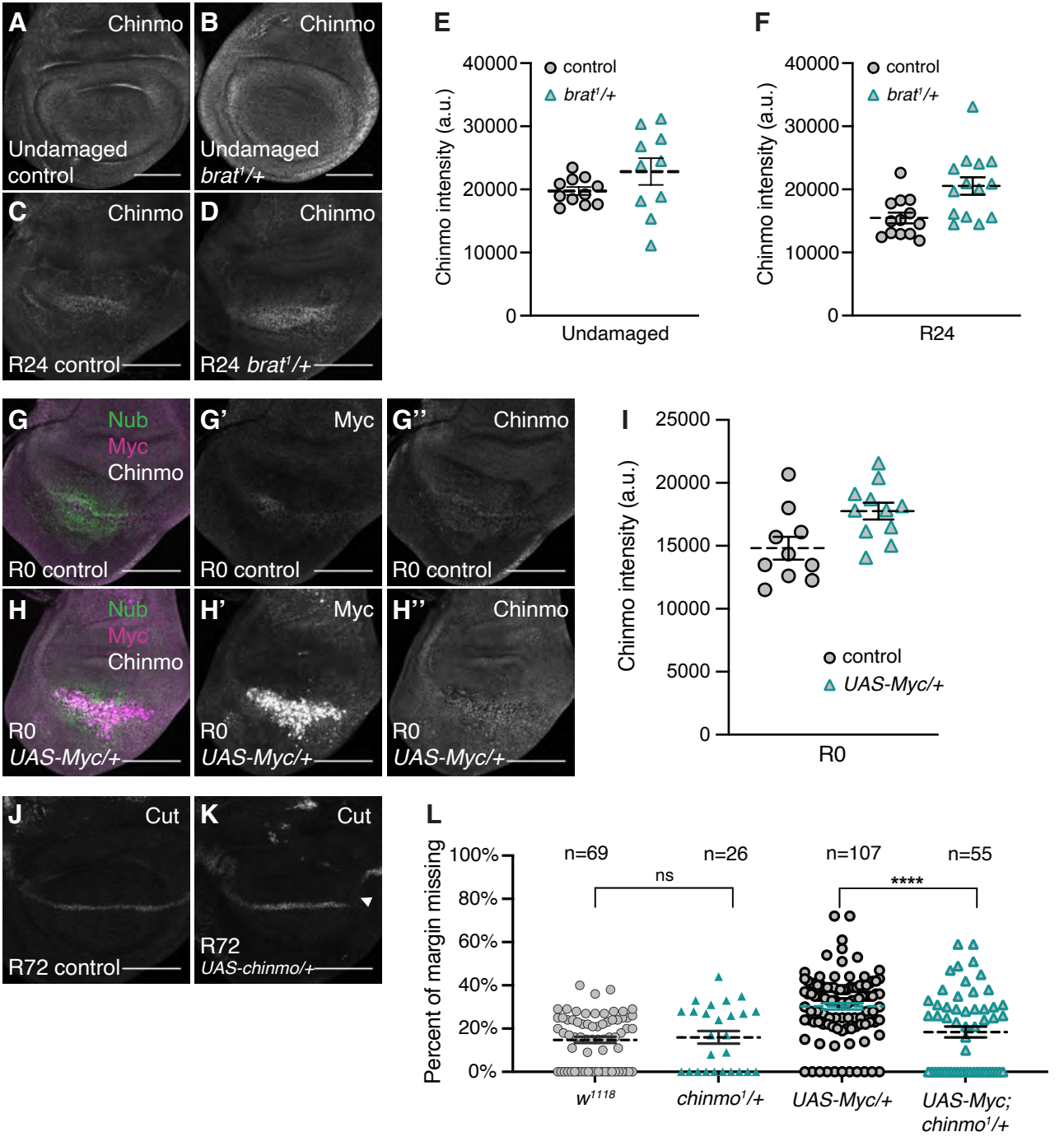
A
Chinmo
Undamaged
control
B
Chinmo
Undamaged
brat¹/+
C
Chinmo
R24 control
D
Chinmo
R24 brat¹/+
E
Chinmo intensity (a.u.)
40000
30000
20000
10000
0
control
brat¹/+
Undamaged
F
Chinmo intensity (a.u.)
40000
30000
20000
10000
0
control
brat¹/+
R24
G
Nub
Myc
Chinmo
R0 control
G'
Myc
R0 control
G''
Chinmo
R0 control
H
Nub
Myc
Chinmo
R0
UAS-Myc/+
H'
Myc
R0
UAS-Myc/+
H''
Chinmo
R0
UAS-Myc/+
I
Chinmo intensity (a.u.)
25000
20000
15000
10000
5000
0
control
UAS-Myc/+
R0
J
Cut
R72 control
K
Cut
R72
UAS-chinmo/+
L
Percent of margin missing
100%
80%
60%
40%
20%
0%
n=69
n=26
n=107
n=55
ns
****
w¹¹¹⁸
chinmo¹/+
UAS-Myc/+
UAS-Myc;
chinmo¹/+

1063 **Figure 7. Chinmo levels are elevated in *brat*^{1}/+ and Myc-overexpressing**
1064 **regenerating discs.**

1065 (A-B) Anti-Chinmo immunostaining in an undamaged control (w^{1118}) disc (A) and an
1066 undamaged *brat*^{1}/+ disc (B). (C-D) Anti-Chinmo immunostaining in an R24 control
1067 (w^{1118}) disc (C) and an R24 *brat*^{1}/+ disc (D). (E) Quantification of Chinmo fluorescence
1068 intensity in undamaged control (w^{1118}) (n = 11) and undamaged *brat*^{1}/+ (n = 10) discs.
1069 p=0.16 (F) Quantification of Chinmo fluorescence intensity in R24 control (w^{1118}) (n =
1070 13) and R24 *brat*^{1}/+ (n = 14) discs. $p < 0.006$. Area for fluorescence intensity
1071 measurement was defined by the elevated Chinmo expression domain in the wing
1072 pouch. (G) Merge of anti-Nubbin, anti-Myc and anti-Chinmo immunostaining in an R0
1073 control (w^{1118}) disc. (G'-G'') Same disc as (G) showing anti-Myc and anti-Chinmo
1074 immunostaining, respectively. (H) Merge of anti-Nubbin, anti-Myc and anti-Chinmo
1075 immunostaining in an R0 *brat*^{1}/+ disc. (H'-H'') Same disc as (H) showing anti-Myc and
1076 anti-Chinmo immunostaining, respectively. (I) Quantification of Chinmo fluorescence
1077 intensity in R0 control (w^{1118}) (n = 10) and R0 *UAS-Myc/*+ (n = 11) discs. $p < 0.02$. Area
1078 for fluorescence intensity measurement was defined by the elevated Myc expression
1079 domain in the wing pouch. (J-K) Anti-Cut immunostaining in control (J) and UAS-chinmo
1080 (K) R72 discs. Arrowhead shows missing Cut expression in K. (L) Margin tissue lost as
1081 a percentage of total wing perimeter for control (w^{1118}) (n = 69), *chinmo*^{1}/+ *(n=26),*
1082 *UAS-Myc/*+ (n = 107) *,* and *UAS-Myc/+; chinmo*^{1}/+ (n=55) wings. ****p = 9.11E-05. Error
1083 bars represent SEM. Student's T-test used for statistical analyses. Scale bars are 100
1084 µm.

Figure 8

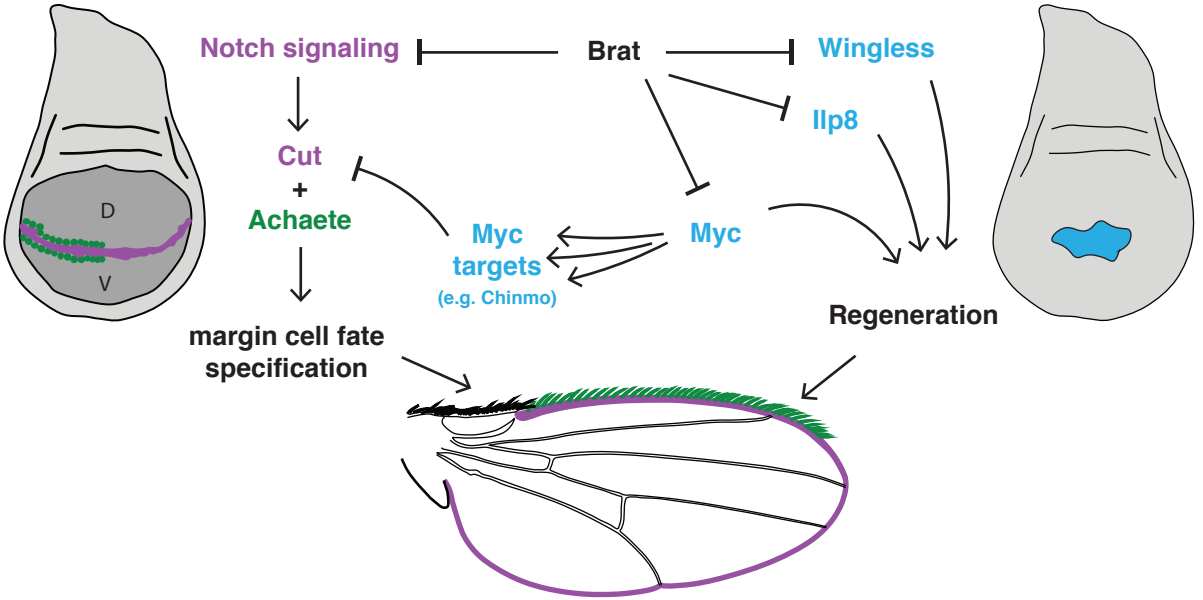
D
V
Notch signaling
Brat
Wingless
Ilp8
Cut
+
Achaete
Myc
targets
(e.g. Chinmo)
Myc
Regeneration
margin cell fate
specification

1085 **Figure 8. Brat restricts pro-regeneration factors and ensures correct margin cell-**

1086 **fate specification.**

1087 Model describing the network of Brat targets in the regenerating wing imaginal disc.

1088 Importantly, Brat restricts Myc levels, limiting expression of Myc's targets, including

1089 Chinmo, to allow correct margin cell-fate specification.

Figure S1

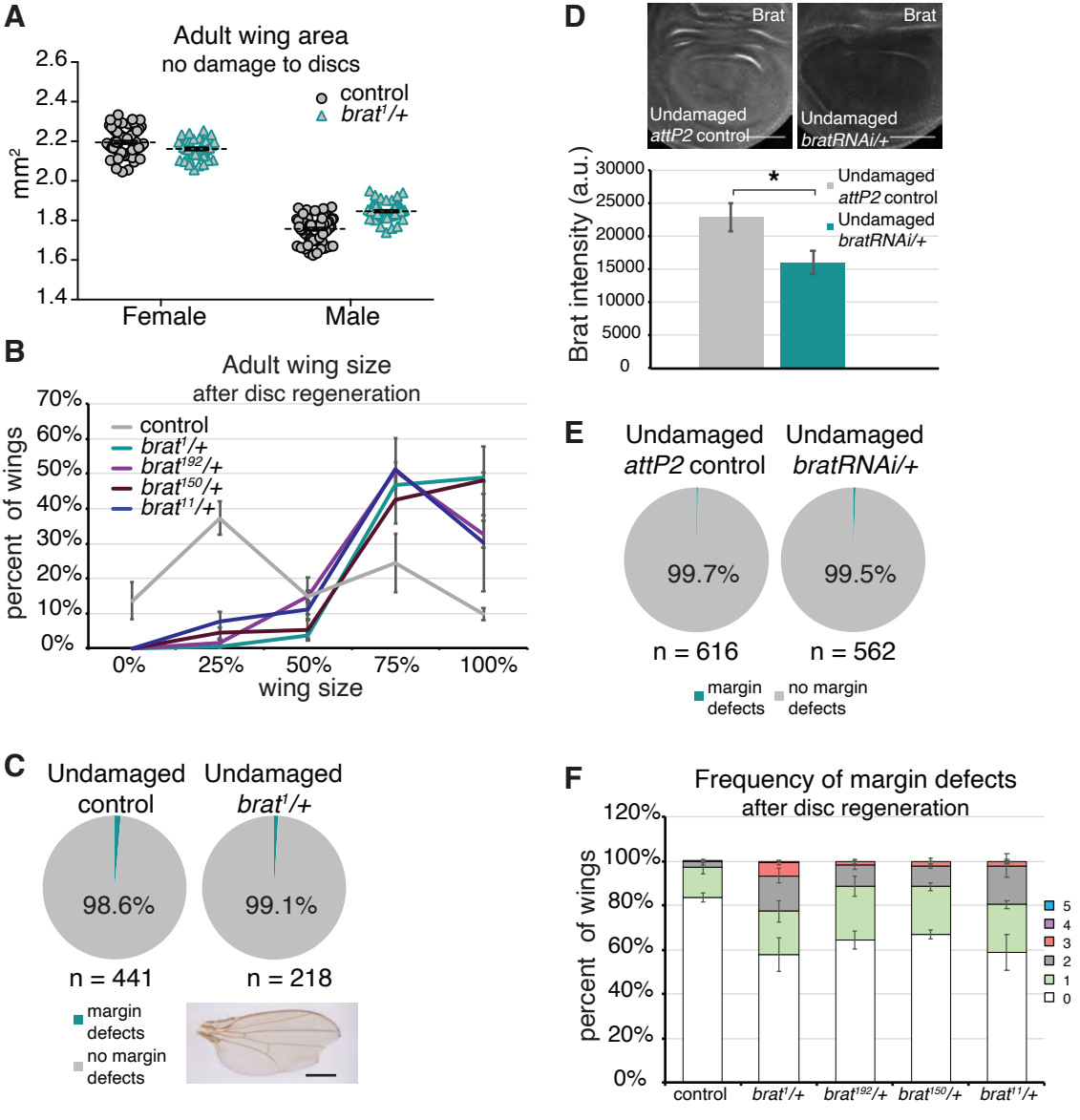
A
Adult wing area
no damage to discs
control
brat1/+
mm2
2.6
2.4
2.2
2.0
1.8
1.6
1.4
Female
Male
B
Adult wing size
after disc regeneration
control
brat1/+
brat192/+
brat150/+
brat11/+
percent of wings
70%
60%
50%
40%
30%
20%
10%
0%
0%
25%
50%
75%
100%
wing size
C
Undamaged control
Undamaged brat1/+
98.6%
99.1%
n = 441
n = 218
margin defects
no margin defects
D
Brat
Brat
Undamaged attP2 control
Undamaged bratRNAi/+
Brat intensity (a.u.)
30000
25000
20000
15000
10000
5000
0
*
Undamaged attP2 control
Undamaged bratRNAi/+
E
Undamaged attP2 control
Undamaged bratRNAi/+
99.7%
99.5%
n = 616
n = 562
margin defects
no margin defects
F
Frequency of margin defects
after disc regeneration
percent of wings
120%
100%
80%
60%
40%
20%
0%
control
brat1/+
brat192/+
brat150/+
brat11/+
5
4
3
2
1
0

1090 **Figure S1. Reduction of *brat* expression does not cause enhanced growth or**

1091 **margin defects during normal development (Related to Figure 1).**

1092 (A) Adult wing area measured using ImageJ after mounting and imaging wings, for

1093 undamaged control (w^{1118}) (n = 63 female and 70 male) and $brat^{1}$/+ (n = 38 female and

1094 48 male) wings. *rnGAL4, GAL80^{ts}/TM6B* females were crossed to w^{1118} or $brat^{1}$/*SM6-*

1095 *TM6B* males and taken through the protocol shown in Figure 1A. (B) Adult wing sizes

1096 after disc regeneration for control (w^{1118}) (n = 599), $brat^{1}$/+ (n = 199), $brat^{192}$/+ (n = 237),

1097 $brat^{150}$/+ (n = 235) and $brat^{11}$/+ (n = 188) wings, from three independent experiments.

1098 (C) Margin defects detected in adult wings from undamaged control (w^{1118}) and $brat^{1}$/+

1099 discs. *rnGAL4, GAL80^{ts}/TM6B* females were crossed to w^{1118} or $brat^{1}$/*SM6-TM6B* males

1100 and taken through the protocol shown in Figure 1A. Margin defects detected in the

1101 undamaged wings were never as severe as the ones seen in $brat^{1}$/+ wings after disc

1102 regeneration. A representative wing with margin defects is shown. (D) Anti-Brat

1103 immunostaining in undamaged control (*attP2*) and *bratRNAi/*+ discs. *rnGAL4,*

1104 *GAL80^{ts}/TM6B* females were crossed to *attP2* or *bratRNAi* males. Larvae were kept at

1105 18°C and shifted to 30°C on day 7 AEL. Discs were dissected 24 hours after the shift to

1106 30°C. Quantification of Brat fluorescence intensity in undamaged control *(attP2*) (n = 15)

1107 and *bratRNAi*/+ (n = 15) discs. Area for fluorescence intensity measurement was

1108 defined by wing pouch morphology and Anti-Myc co-immunostaining. * p = 0.02. (E)

1109 Margin defects detected in adult wings from undamaged control (*attP2*) and *bratRNAi*

1110 dics. *rnGAL4, GAL80^{ts}/TM6B* females were crossed to *attP2* or *bratRNAi* males. Larvae

1111 were kept at 18°C and shifted to 30°C on day 7 AEL and kept there until eclosion. (F)

1112 Frequency of margin defects seen in adult wings after disc regeneration for control

1113 (w^{1118}) (n = 240), $brat^{1}$/+ (n = 191), $brat^{192}$/+ (n = 196), $brat^{150}$/+ (n = 213) and $brat^{11}$/+ (n

1114 = 152) wings. Wings in (G) are from the same experiments as (B). Error bars represent

1115 SEM. Student's T-test used for statistical analyses. Scale bars are 100 μm. Scale bars

1116 for adult wings are 0.5 mm.

Figure S2

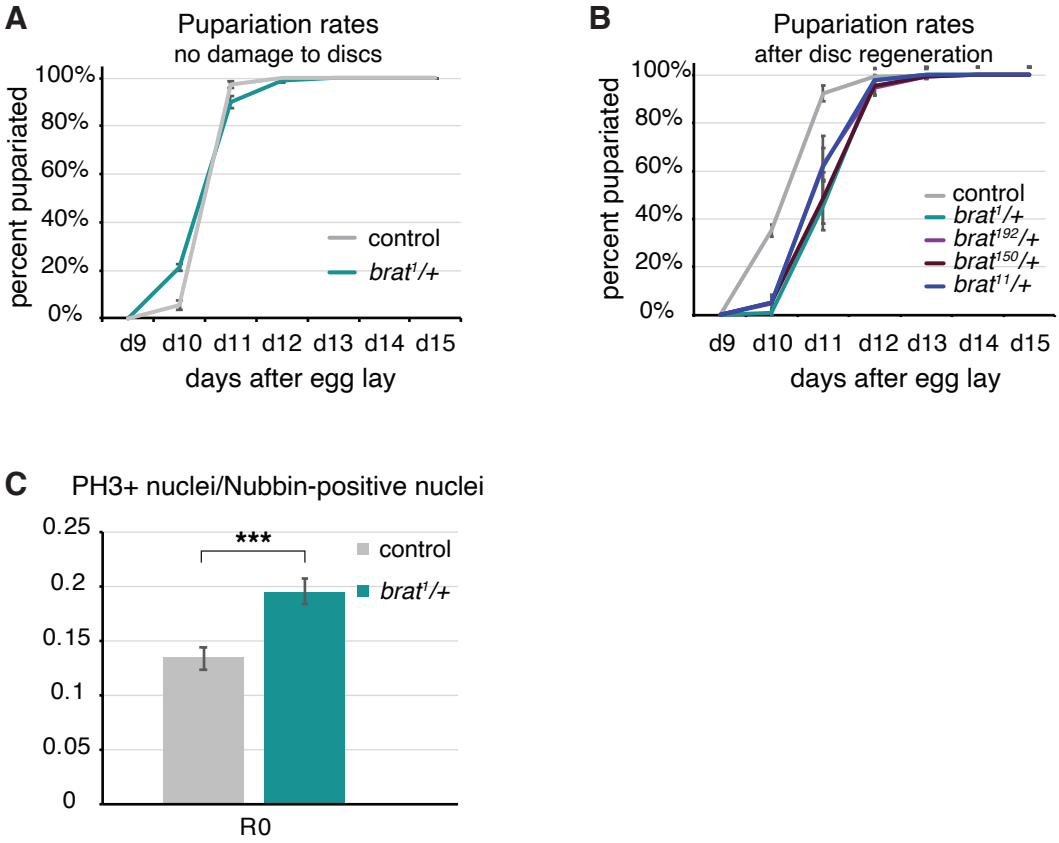
A
Pupariation rates
no damage to discs
percent pupariated
100%
80%
60%
40%
20%
0%
d9 d10 d11 d12 d13 d14 d15
days after egg lay
control
brat1/+
B
Pupariation rates
after disc regeneration
percent pupariated
100%
80%
60%
40%
20%
0%
d9 d10 d11 d12 d13 d14 d15
days after egg lay
control
brat1/+
brat192/+
brat150/+
brat11/+
C
PH3+ nuclei/Nubbin-positive nuclei
0.25
0.2
0.15
0.1
0.05
0
***
control
brat1/+
R0

1117 **Figure S2. Reduction of *brat* expression delays pupariation in a regeneration-**

1118 **specific manner (Related to Figure 2).**

1119 (A) Pupariation rates in undamaged control (w^{1118}) (n = 221) and $brat^{1}$/+ (n = 110)

1120 animals, from three independent experiments. (B) Pupariation rates after disc

1121 regeneration for control (w^{1118}) (n = 384), $brat^{1}$/+ (n = 107), $brat^{192}$/+ (n = 131), $brat^{150}$/+

1122 (n = 114) and $brat^{11}$/+ (n = 113) animals. Pupariation rates are from the same

1123 experiments as in Figure 2A. (C) PH3-positive nuclei were counted within the

1124 regenerating tissue as marked by Anti-Nubbin co-immunostaining. Total number of

1125 nuclei were also counted in the Nubbin expressing region. Ratio of PH3-positive nuclei

1126 and total Nubbin-positive nuclei for control (w^{1118}) and $brat^{1}$/+ discs at R0 (n = 16 and

1127 18). *** $p < 0.0005$. Error bars represent SEM. Student's T-test used for statistical

1128 analyses. Error bars represent SEM.

Figure S3

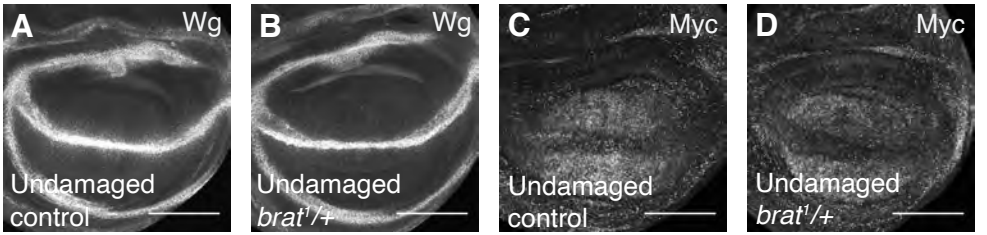
A
Wg
Undamaged
control
B
Wg
Undamaged
brat1/+
C
Myc
Undamaged
control
D
Myc
Undamaged
brat1/+

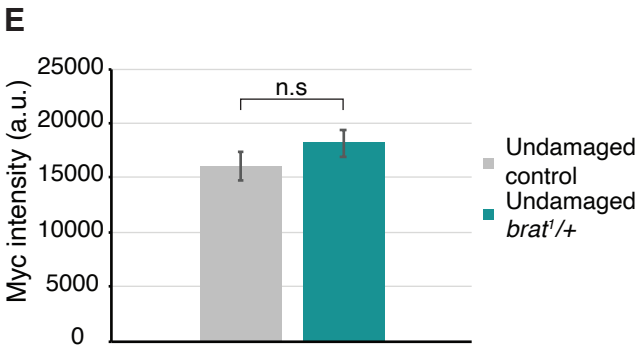
E
Myc intensity (a.u.)
25000
20000
15000
10000
5000
0
n.s
Undamaged
control
Undamaged
brat1/+

1129 **Figure S3. Effects of reduced Brat on Wg and Myc expression are regeneration**

1130 **specific (Related to Figure 3).**

1131 (A-B) Anti-Wg immunostaining in an undamaged control (w^{1118}) disc (A) and an

1132 undamaged $brat^{1}$/+ disc (B). (C-D) Anti-Myc immunostaining in an undamaged control

1133 (w^{1118}) disc (C) and an undamaged $brat^{1}$/+ disc (D). (E) Quantification of Myc

1134 fluorescence intensity in undamaged control (w^{1118}) (n = 10) and $brat^{1}$/+ (n = 10) discs.

1135 Area for fluorescence intensity measurement was defined by wing pouch morphology

1136 and the elevated Myc expression domain in the wing pouch. Error bars represent SEM.

1137 Student's T-test used for statistical analyses. Scale bars are 100 μm.

Figure S4

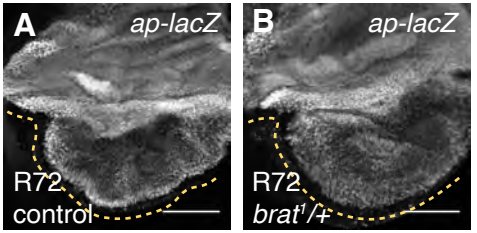
A
ap-lacZ
R72
control

B
ap-lacZ
R72
brat1/+

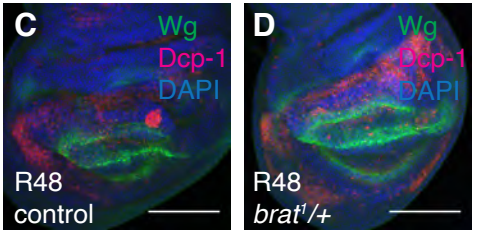
C
Wg
Dcp-1
DAPI
R48
control
D
Wg
Dcp-1
DAPI
R48
brat1/+

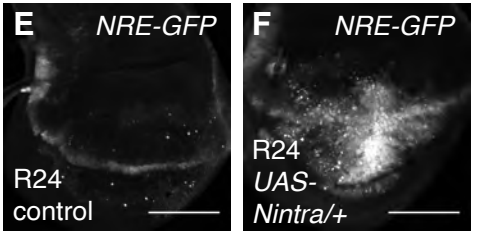
E
NRE-GFP
R24
control
F
NRE-GFP
R24
UAS-
Nintra/+

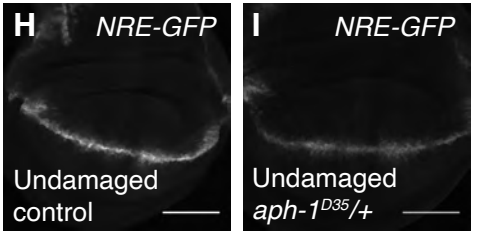
H
NRE-GFP
Undamaged
control
I
NRE-GFP
Undamaged
aph-1D35/+

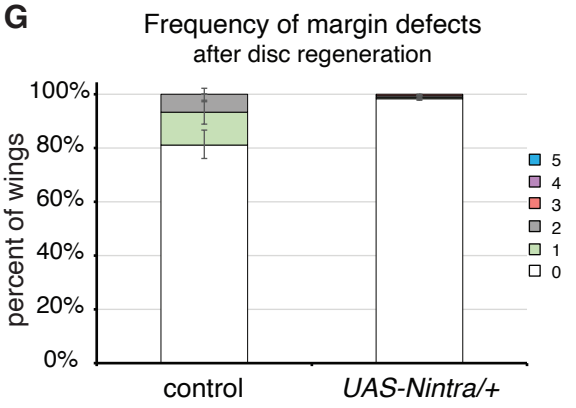
G
Frequency of margin defects
after disc regeneration
percent of wings
100%
80%
60%
40%
20%
0%
control
UAS-Nintra/+
5
4
3
2
1
0

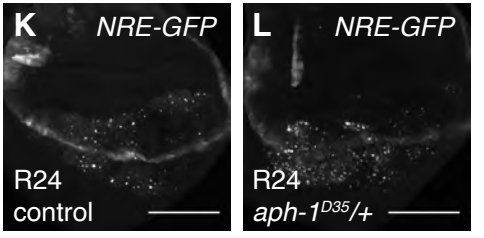
K
NRE-GFP
R24
control
L
NRE-GFP
R24
aph-1D35/+

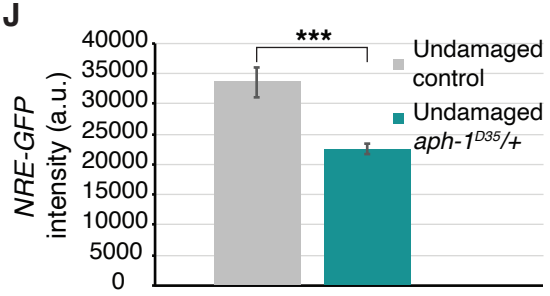
J
NRE-GFP
intensity (a.u.)
40000
35000
30000
25000
20000
15000
10000
5000
0
***
Undamaged
control
Undamaged
aph-1D35/+

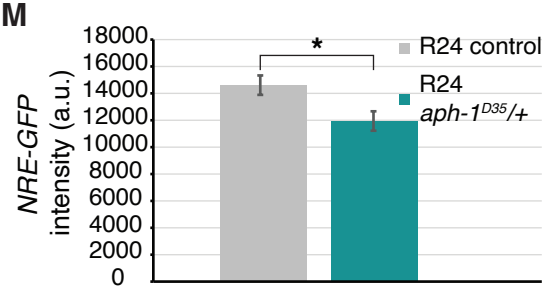
M
NRE-GFP
intensity (a.u.)
18000
16000
14000
12000
10000
8000
6000
4000
2000
0
*
R24 control
R24
aph-1D35/+

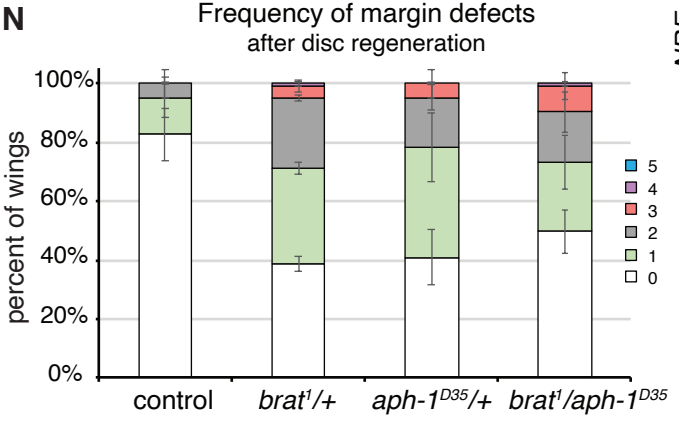
N
Frequency of margin defects
after disc regeneration
percent of wings
100%
80%
60%
40%
20%
0%
control
brat1/+
aph-1D35/+
brat1/aph-1D35
5
4
3
2
1
0

1138 **Figure S4. Elevated Notch signaling does not cause margin defects (Related to**

1139 **Figure 4).**

1140 (A-B) *ap-lacZ* expression in an R72 control (w^{1118}) disc (A) and an R72 $brat^{1}$/+ disc (B).

1141 Dashed yellow lines are drawn next to the DV boundary to highlight it. (C-D) Anti-Wg

1142 (green) and anti-cleaved Dcp1 (red) immunostaining in an R48 control (w^{1118}) disc (C)

1143 and an R48 $brat^{1}$/+ disc (D). (E-F) *NRE-GFP* expression in an R24 control (w^{1118}) disc

1144 (E) and an R24 *UAS-Nintra/*+ disc (F). (G) Frequency of margin defects seen in adult

1145 wings after disc regeneration for control (w^{1118}) (n = 84) and *UAS-Nintra/*+ (n = 357)

1146 wings, from five independent experiments. (H-I) *NRE-GFP* expression in an undamaged

1147 control (w^{1118}) disc (H) and an undamaged *aph-1*^{D35}/+ disc (I). *NRE-GFP*/+ and *NRE-*

1148 *GFP*/*aph-1*^{D35} animals were raised at room temperature and dissected during third

1149 instar. (J) Quantification of GFP intensity in undamaged control (w^{1118}) (n = 15) and *aph-*

1150 *1*^{D35}/+ (n = 15) discs. *** $p < 0.0006$. (K-L) *NRE-GFP* expression in an R24 control

1151 (w^{1118}) disc (K) and an R24 *aph-1*^{D35}/+ disc (L). (M) Quantification of GFP intensity in

1152 R24 control (w^{1118}) (n = 13) and R24 *aph-1*^{D35}/+ (n = 11) discs. * $p < 0.02$. (N)

1153 Frequency of margin defects in adult wings after disc regeneration for control (w^{1118}) (n

1154 = 21), $brat^{1}$/+ (n = 137), *aph-1*^{D35}/+ (n = 38) and $brat^{1}$/*aph-1*^{D35}(n = 80) wings. Error bars

1155 represent SEM. Student's T-test used for statistical analyses. Scale bars are 100 μm.

Figure S5

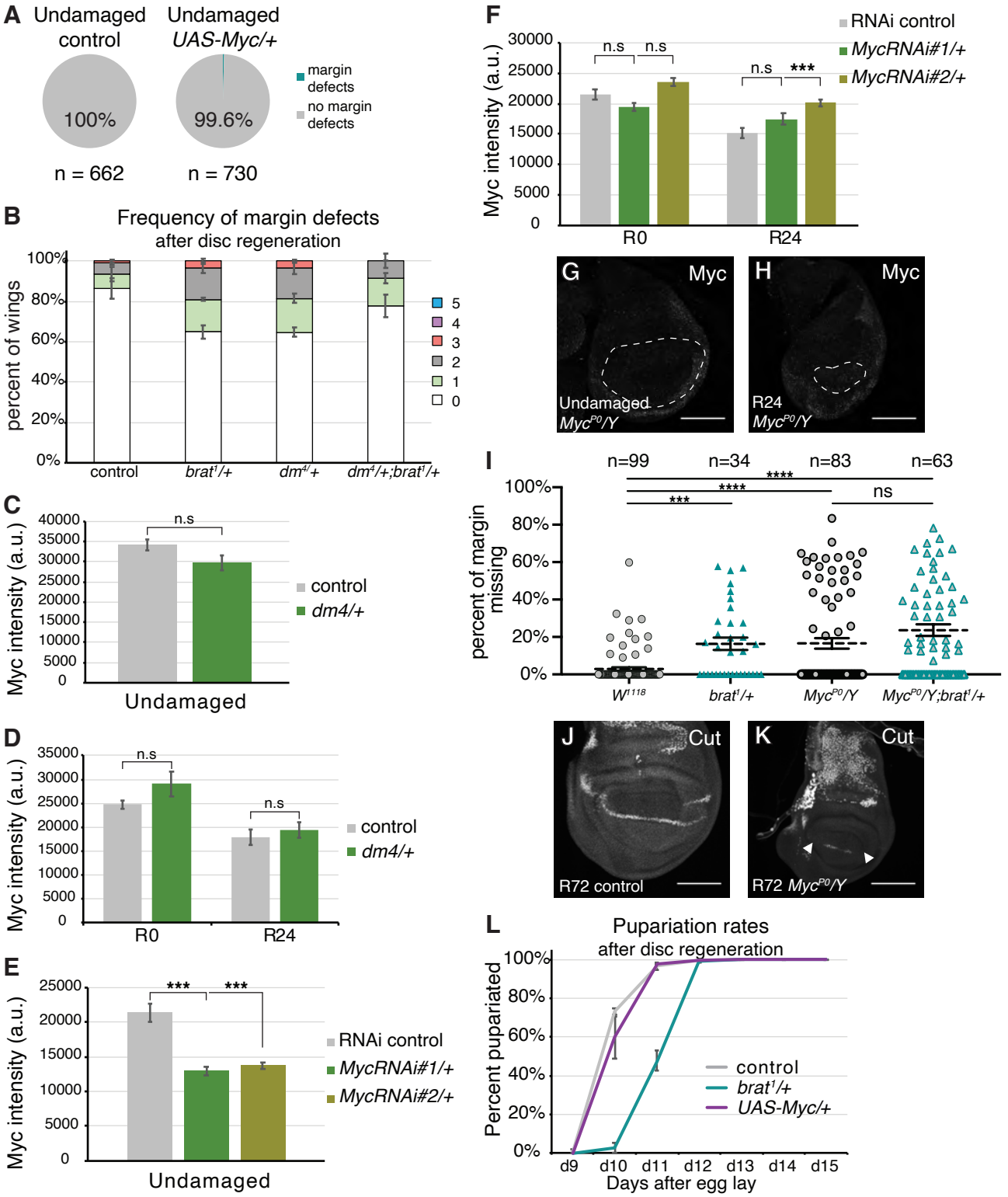
A
Undamaged control
Undamaged UAS-Myc/+
100%
99.6%
margin defects
no margin defects
n = 662
n = 730
B
Frequency of margin defects after disc regeneration
percent of wings
100%
80%
60%
40%
20%
0%
control
brat1/+
dm4/+
dm4/+;brat1/+
5
4
3
2
1
0
C
Myc intensity (a.u.)
n.s
control
dm4/+
Undamaged
D
Myc intensity (a.u.)
n.s
n.s
control
dm4/+
R0
R24
E
Myc intensity (a.u.)
***
***
RNAi control
MycRNAi#1/+
MycRNAi#2/+
Undamaged
F
Myc intensity (a.u.)
n.s
n.s
n.s
***
RNAi control
MycRNAi#1/+
MycRNAi#2/+
R0
R24
G
Myc
Undamaged
MycP0/Y
H
Myc
R24
MycP0/Y
I
n=99
n=34
n=83
n=63
****
****
***
ns
percent of margin missing
W1118
brat1/+
MycP0/Y
MycP0/Y;brat1/+
J
Cut
R72 control
K
Cut
R72 MycP0/Y
L
Pupariation rates after disc regeneration
Percent pupariated
control
brat1/+
UAS-Myc/+
d9
d10
d11
d12
d13
d14
d15
Days after egg lay

1156 **Figure S5. Reduction of Myc expression during regeneration also disrupts margin**
1157 **fate specification (Related to Figure 5).**

1158 (A) Margin defects detected in adult wings from undamaged control (w^{1118}) and *UAS-*
1159 *Myc/+* discs. *rnGAL4, GAL80^{ts}/TM6B* females were crossed to w^{1118} or *UAS-Myc* males
1160 and taken through the protocol shown in Figure 1A. (B) Frequency of margin defects in
1161 adult wings after disc regeneration for control (w^{1118}) (n = 103), *brat^{1}/+* (n = 203), *dm^{4}/+*
1162 (n = 94) and *dm^{4}/+; brat^{1}/+* (n = 94) wings, from three independent experiments. (C)
1163 Quantification of Myc fluorescence intensity in undamaged control (w^{1118}) (n = 12) and
1164 *dm^{4}/+* (n = 11) discs. w^{1118} males were crossed to w^{1118} or *dm^{4}/FM7i, ActGFP* females
1165 and dissected when the animals were third instar. Area for fluorescence intensity
1166 measurement was defined by wing pouch morphology and the elevated Myc expression
1167 domain in the wing pouch. (D) Quantification of Myc fluorescence intensity in R0 control
1168 (w^{1118}) (n = 13), R0 *dm^{4}/+* (n = 10), R24 control (w^{1118}) (n = 13), and R24 *dm^{4}/+* (n = 10)
1169 discs. Area for fluorescence intensity measurement was defined by the elevated Myc
1170 expression domain in the wing pouch. (E) Quantification of Myc fluorescence intensity in
1171 undamaged control (VDRC genetic background line, called control) (n = 14),
1172 *MycRNAi#1/+* (n = 12), and *MycRNAi#2/+* (n = 13) discs. *rnGAL4, GAL80^{ts}/TM6B*
1173 females were crossed to the control, *MycRNAi#1*, or *MycRNAi#2* males. The animals
1174 were shifted to 30°C during early third instar and kept there for 28 hours then dissected.
1175 *MycRNAi#1/+* *** $p < 0.000007$, *MycRNAi#2/+* *** $p < 0.00002$. Area for fluorescence
1176 intensity measurement was defined by wing pouch morphology. (F) Quantification of
1177 Myc fluorescence intensity in R0 control (n = 13), R0 *MycRNAi#1/+* (n = 15), R0
1178 *MycRNAi#2/+* (n = 13), R24 control (n = 13), R24 *MycRNAi#1/+* (n = 13), and R24

1179 *MycRNAi#2/+* (n = 13) discs. Fluorescence intensity was measured in the area marked
1180 by Anti-Nubbin immunostaining. *** $p < 0.00007$. (G,H) Anti-Myc immunostaining in
1181 undamaged (G) and regenerating R24 (H) Myc^{P0}/Y imaginal wing discs. Dashed line
1182 outlines the wing pouch defined by anti-Nubbin immunostaining. (I) Margin tissue lost as
1183 a percentage of total wing perimeter for adult wings after disc damage and regeneration
1184 in the noted genotypes. (J, K) Immunostaining for Cut in control (J) and Myc^{P0}/Y (K)
1185 regenerated (R72) discs showing margin disruption in the mutants.(L) Pupariation rates
1186 after disc regeneration for control (w^{1118}) (n = 216), $brat^{1}/+$ (n = 114) and *UAS-Myc/+* (n
1187 = 209) animals, from three independent experiments. Error bars represent SEM.
1188 Student's T-test used for statistical analyses.

Figure S6

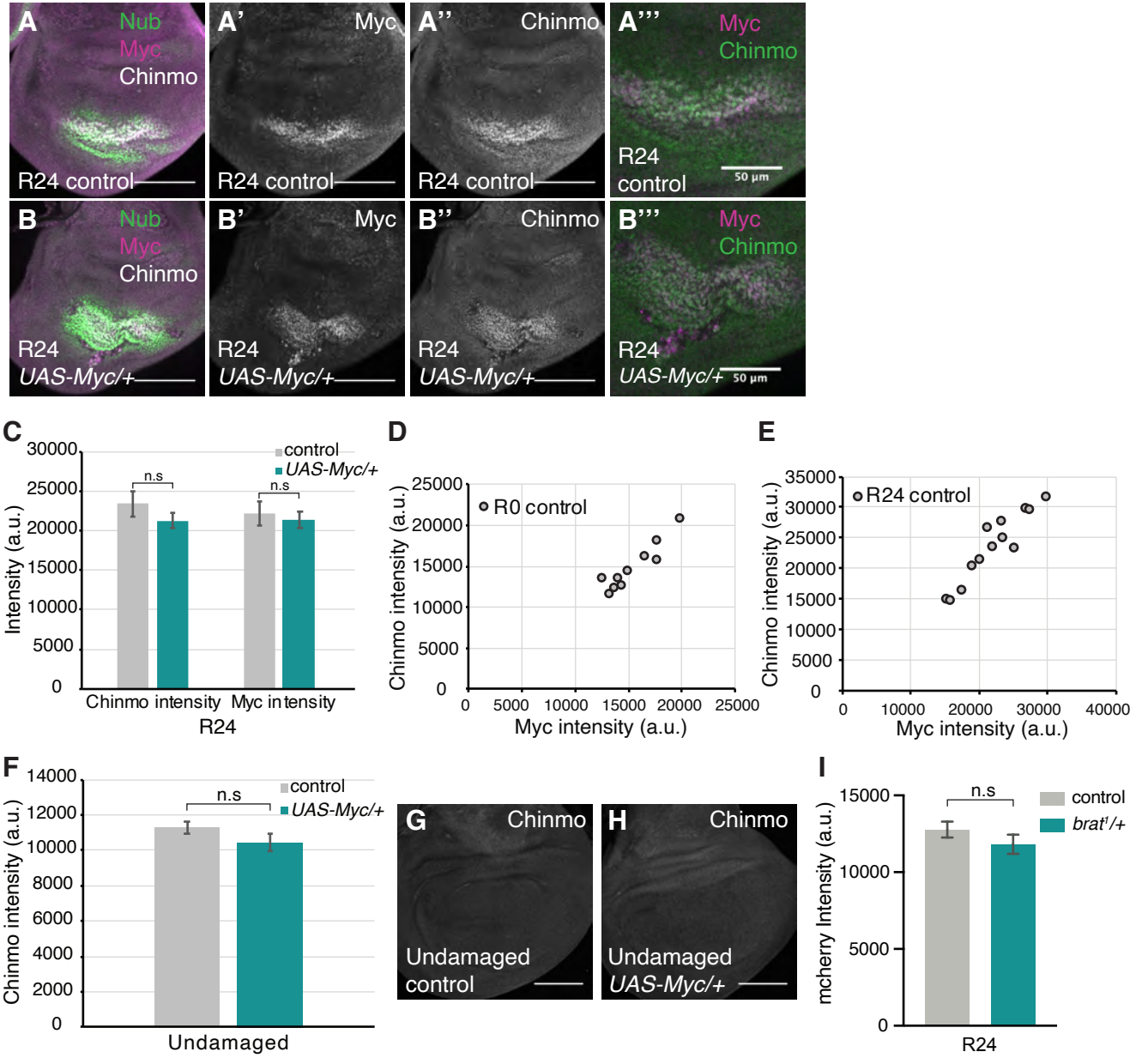
A
Nub
Myc
Chinmo
R24 control
A'
Myc
R24 control
A''
Chinmo
R24 control
A'''
Myc
Chinmo
R24
control
50 µm
B
Nub
Myc
Chinmo
R24
UAS-Myc/+
B'
Myc
R24
UAS-Myc/+
B''
Chinmo
R24
UAS-Myc/+
B'''
Myc
Chinmo
R24
UAS-Myc/+
50 µm
C
control
UAS-Myc/+
n.s
n.s
Intensity (a.u.)
Chinmo intensity
Myc intensity
R24
D
R0 control
Chinmo intensity (a.u.)
Myc intensity (a.u.)
E
R24 control
Chinmo intensity (a.u.)
Myc intensity (a.u.)
F
control
UAS-Myc/+
n.s
Chinmo intensity (a.u.)
Undamaged
G
Chinmo
Undamaged
control
H
Chinmo
Undamaged
UAS-Myc/+
I
control
brat1/+
n.s
mcherry Intensity (a.u.)
R24

1189 **Figure S6. Myc regulates Chinmo expression (Related to Figure 7).**

1190 (A) Merge of anti-Nubbin, anti-Myc and anti-Chinmo immunostaining in an R24 control
1191 (w^{1118}) disc. (A'-A'') Same disc as (A) showing anti-Myc and anti-Chinmo
1192 immunostaining, respectively. (A''') Same disc as (A) showing an enlarged merge of
1193 anti-Myc and anti-Chinmo immunostaining. (B) Merge of anti-Nubbin, anti-Myc and anti-
1194 Chinmo immunostaining in an R24 *UAS-Myc/*+ disc. (B'-B'') Same disc as (B) showing
1195 anti-Myc and anti-Chinmo immunostaining, respectively. (B''') Same disc as (B) showing
1196 an enlarged merge of anti-Myc and anti-Chinmo immunostaining. (C) Quantification of
1197 Chinmo and Myc fluorescence intensity in R24 control (w^{1118}) (n = 13) and R24 *UAS-*
1198 *Myc/*+ (n = 14) discs. Area for fluorescence intensity measurement was defined by the
1199 elevated Myc expression domain in the wing pouch. Note that Myc and Chinmo
1200 expression co-localize. (D-E) Scatter plot showing correlation between Myc and Chinmo
1201 expression levels at R0 (D) and R24 (E). Pearson correlation coefficient for R0 = 0.93
1202 and R24 = 0.94. (F) Quantification of Chinmo fluorescence intensity in undamaged discs
1203 dissected 31 hours after animals were shifted to 30°C on day 7 AEL. Control (+ *;*
1204 *rnGAL4,GAL80ts/*+) (n = 14) and *UAS-Myc (UAS-Myc/*+ *; rnGAL4, GAL80ts/*+*)* (n = 14).
1205 Area for fluorescence intensity measurement was defined by the Myc expression
1206 domain in the wing pouch. (G-H) Anti-Chinmo immunostaining in an undamaged control
1207 disc (G) and an undamaged *UAS-Myc/*+ disc (H). (I) Quantification of fluorescence
1208 intensity from the *UAS-mCherry-chinmoUTR* transgene in control (n=16) and brat/+
1209 (n=15) R24 regenerating discs. Area for fluorescence intensity measurement was
1210 defined by Nubbin expression. Error bars represent SEM. Student's T-test used for
1211 statistical analyses. Scale bars are 100 μm, unless stated otherwise.